Università degli Studi di Padova

Departement Of Industrial Engineering

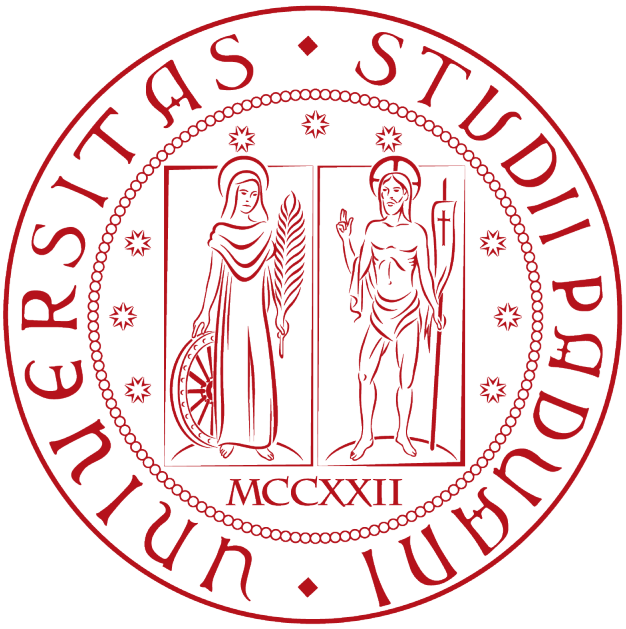

Master Degree In Aerospace Engineering

Wall Modelled Large Eddy Simulation of hypersonic turbulent boundary layer

---

Thesis Advisor:

Ing. **Francesco De Vanna,** PhD

Candidate:

Gabriele Peterle

MATR. 1237230

Thesis Co-advisor:

Ing. **Michele Cogo**

Prof. **Francesco Picano**

To my family, to my girlfriend and to all those who helped me during these hard years.

Abstract

This thesis deals with the numerical simulation of an hypersonic turbulent flow on a flat plate with a temperature gradient. The simulations were made by using URANOS.
In particular, the task is to validate the code and find criticalities and parameters that affect the final solution.
The experiments provide a comparison between DNS data (by Zang), LES data and WM-LES simulations. More specifically, the mean velocity profiles, velocity fluctuations (Reynolds Stresses) and friction coefficient along x and y directions are compared.
In order to do that, different techniques and various grids have been used, then we evaluated how the solutions change as these parameters vary.
The reason lies in validating a technique that is increasingly interesting for the accuracy it can provide with a very low computational cost when compared to other techniques available nowadays.

Sommario

In questa tesi viene proposta una campagna di simulazioni numeriche di un flusso ipersonico turbolento su una lastra piana con gradiente di temperatura. Le simulazioni sono state condotte numericamente tramite URANOS.
In particolare lo scopo è validare il codice ed individuare criticità e/o parametri che più influenzano la soluzione.
La campagna sperimentale prevede il confronto tra dati DNS (proposti da Zang), dati LES e simulazioni WMLES. Più precisamente si confrontano tra di loro i profili di velocità medi, le fluttuazioni (stress di Reynolds) e coefficiente d'attrito lungo le direzioni x e y.
Per fare questo sono stati utilizzati diversi modelli e diverse griglie e se ne è valutato poi come cambiano le soluzioni al variare di questi parametri.
Il motivo risiede nel validare una tecnica che risulta sempre più interessante per l'accuratezza che può fornire tramite un costo computazionale molto ridotto se confrontato con altre tecniche ora disponibili.

Acknowledgements

First of all, I would like to thank Ing. Francesco De Vanna (PhD) for the opportunity and for his support during these last months, professor Francesco Picano and Ing. Michele Cogo for guiding me through this work and for everything they taught me. I am grateful to my family for all the support they gave me. Thanks to my girlfriend Emma for sharing this journey with me through the good and the bad times. Thanks to all my friends for being the best friends I could ever wish for.

Contents

Chapter 1

Introduction

1.1 Hypersonic Flows

Hypersonic flows are particular flow fields in which the fluid velocity is much higher than the speed of sound, more specifically, we are considering flows with a Mach number which is higher than five. Their behaviour is far from been completely known because there are many issues concerning these flows.
For instance, the high velocity implies high aerodynamic heating and chemical phenomena. This translates into difficulties in predicting the behaviour of the flow and in performing good simulations, which leads to the need of high experimental resources.
The three common ways to study a flow are:

- experimentally
- theoretically
- computationally

The latter is the most used for hypersonic flows, since it allows an accurate design, without needing a physical object but only by simulating a particular field. It also allows you to study some phenomena that cannot be studied due to sensor's accuracy, such as vorticity, fluctuation, vortex and so on.
Nothing is perfect, and computational studies have their own problems too. In particular, a code is affected by precision errors and computational cost.
The latter is a trouble because although it may be possible to solve a flow field mathematically, in the reality it is not feasible due to the trade off between precision and time of simulation.
The difficulty of studying viscous flows is to predict what happens in a small region near the plate, called boundary layer, in which viscous phenomena are relevant. In addition, hypersonic turbulent flows are strongly affected by heating, in particular, the unstable interactions between flow inertia and the viscous shear force generate numerous unique turbulent phenomena and structures, [13].
The aforementioned structures can be represented as "hairpins vortex" and their behavior is

not fully known, in fact, they can auto-generate to form packets that populate a significant fraction of the boundary layer, even at very high Reynolds numbers. The dynamics of packet formation and the ramifications of organization of coherent structures into larger-scale structures is discussed, [14].
Nowadays, hypersonic flows are becoming more and more interesting due to their applications, which involve from civil to military field. To be more precise, their utility can be seen in space applications as re-entry maneuvers or in hypersonic missiles or hypersonic aircraft.
However, we must consider the consequences of the high temperatures, namely the overheat of the surfaces. In fact, hypersonic structures require a strong framework capable of sustaining big loads and new materials able to resist at high temperatures, high friction and high temperature gradients.
In this study, simulations were done in order to understand better the behaviour of hypersonic flows, starting from a flat plate, the simplest geometry but yet very important. To be more realistic on the simulations, a temperature ratio of $T_{rat} = 0.76$ has been introduced. The reason of this lies in the heat that the surface exchanges with the external fluid, which is important because otherwise there would be an overheating of the surface causing the break of it.

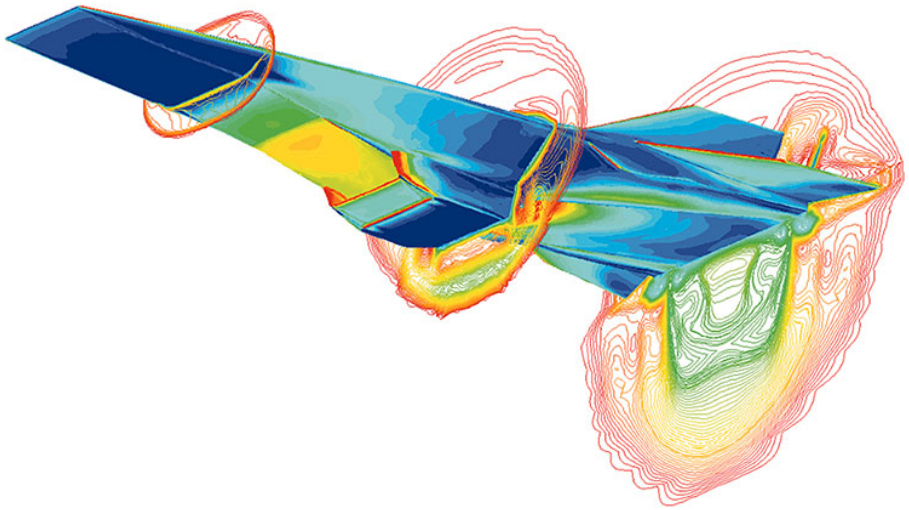

Figure 1.1: NASA X-43, an experimental unmanned hypersonic aircraft, CFD simulation at Mach 7

Furthermore, the flat plate is similar to an external profile of the wing or the external body of some experimental aircraft.
As can be seen in 1.1, the main difference between hypersonic and supersonic flows , beyond being difficult to simulate, are the temperature rises.
This case was studied through a computational way, with the issue of performing correct simulations with a WMLES technique. The WMLES is an approach in which the boundary layer region is not resolved but modeled in a mathematical way, then the outer region is solved. Another improvement is the grid resolution, in particular the grid is uniform and coarse, while

on a LES or DNS technique we have a denser grid. This allows to have good results with a reduced computational cost.

Since we are dealing with turbulent hypersonic flows, we are also considering the problem of turbulence, which has to be studied in a statistical way. Therefore, this thesis solves the problem with some different computational schemes that will be explained in the next chapters.

Chapter 2

BOUNDARY LAYER

2.1 Introduction

The boundary layer is the thin region of flow adjacent to a surface, where the flow is slowed down by the influence of friction between a solid surface and the fluid, in the immediate vicinity the effects of viscosity are significant.
The viscous nature of airflow reduces the local velocities on a surface and is responsible for skin friction. Laminar boundary layers can be classified according to their structure and the circumstances under which they are created:

- laminar boundary layer: represents the case in which the flow is smooth. It is characterized by less skin friction, is also less table then the turbulent case. As the flow goes on the boundary leayer thickness increases.

- turbulent boundary layer: in this case, at a certain distance from the leading edge there is a transition in which the smooth laminar flows breaks down and transitions to a turbulent flow.

2.2 Properties

In order to describe boundary layer it is needed to know the main phisical characteristics such as the Temperature "T", velocity "u", skin friction "τ_w" and so on. In addiction there are 2 boundary conditions imposed at the wall:

- *adherence*: the components of velocities tangent to the wall are zero at the wall
- *impermeability*: the component of the velocity wall-normal is zero at the wall

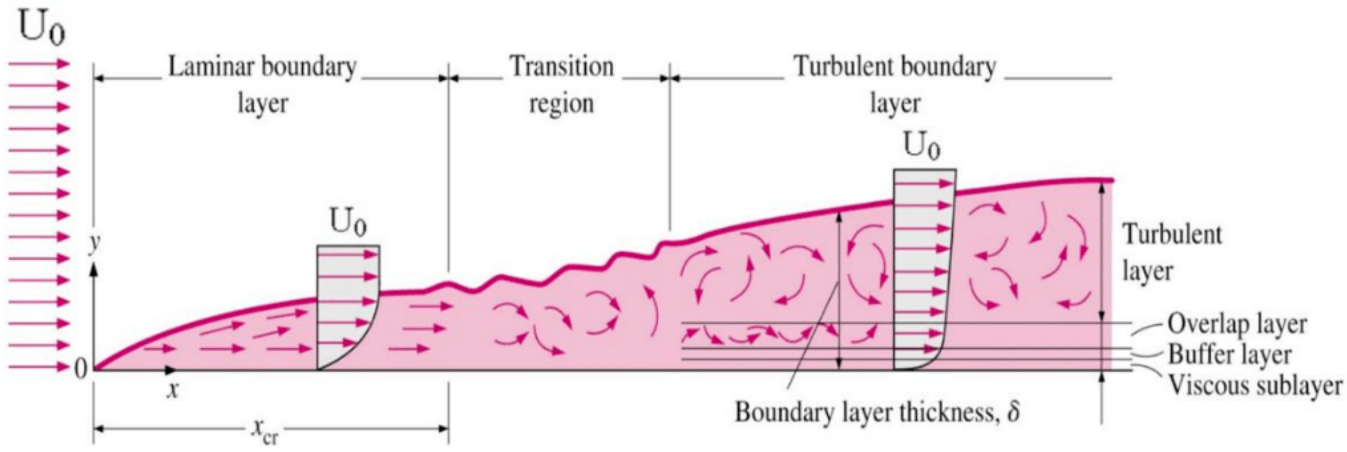

Figure 2.1: General boundary layer

As shown in figure 2.1 this is a general boundary layer, the only way to describe it is to start from Navier-Stokes equations, as descrived on [1]:

$$\frac{\partial u}{\partial x} + \frac{\partial v}{\partial y} = 0 \tag{2.1}$$

$$u\frac{\partial u}{\partial x} + u\frac{\partial v}{\partial y} = -\frac{1}{\rho}\frac{\partial p}{\partial x} + \nu\left(\frac{\partial^2 u}{\partial x^2} + \frac{\partial^2 u}{\partial y^2}\right) \tag{2.2}$$

$$u\frac{\partial v}{\partial x} + v\frac{\partial v}{\partial y} = -\frac{1}{\rho}\frac{\partial p}{\partial y} + \nu\left(\frac{\partial^2 v}{\partial x^2} + \frac{\partial^2 v}{\partial y^2}\right) \tag{2.3}$$

By using the dimensional analysis is possible to estimate the boundary layer thickness along the flat plate, we obtain:

$$\frac{\delta(x)}{x} = \frac{1}{\sqrt{Re_x}} \tag{2.4}$$

This is only an estimation and not an exact solution, there are a lot of ways to calculate the thickness, by knowing this real thickness can be evaluated in several ways:

- δ_{99} : is the distance from the wall in which the velocity u id equal to 99% of the unperturbed velocity.

$$\delta_{99} = y\frac{u}{u_\infty} \tag{2.5}$$

- δ^* : *displacement thickness*. This one is the distance that is have to add to my solution with boundary layer respect to the inviscid one in order to have the same mass flow.

$$\delta^*(x) = \int_0^h \left(1 - \frac{u}{u_\infty}\right) dy \tag{2.6}$$

- θ : *momentum thickness*. It represents the quantity that has to be added to the profile, so that the momentum of the inviscid flow equals the one with boundary layer.

$$\theta(x) = \int_0^h \frac{u}{u_\infty}\left(1 - \frac{u}{u_\infty}\right) dy \tag{2.7}$$

As it can be see in 2.1, the thickness in a flat plate does not varies linearly but in different ways depending on the distance x and each part has his own characteristics. The boundary layer can be divided into 3 regions:

1. In most of the laminar boundary layer thickness grows as:

$$\delta(x) \propto \sqrt{x} \tag{2.8}$$

   Here the solution depends on the boundary conditions and from the initial condition. The behaviour can be studied in 2D.

2. In the transition region $\delta(x)$ remains approximately constant.

3. In the turbulent region. Here instead there is a 3D behaviour, non-stationary and there are swirls or "eddies".

2.3 Turbulent Boundary Layer

In the previous section, we have briefly discussed the incompressible boundary layer theory. However, since this thesis work deals with compressible turbulent flows, it is mandatory to describe the main properties of a turbulent boundary layer. The passage from a laminar to a turbulent boundary layer is not immediate but requires some space where the transition process arises, after which the boundary layer is fully turbulent. The central issues are: the mean velocity profile, frictions laws and the balance equations. In general all the dynamics

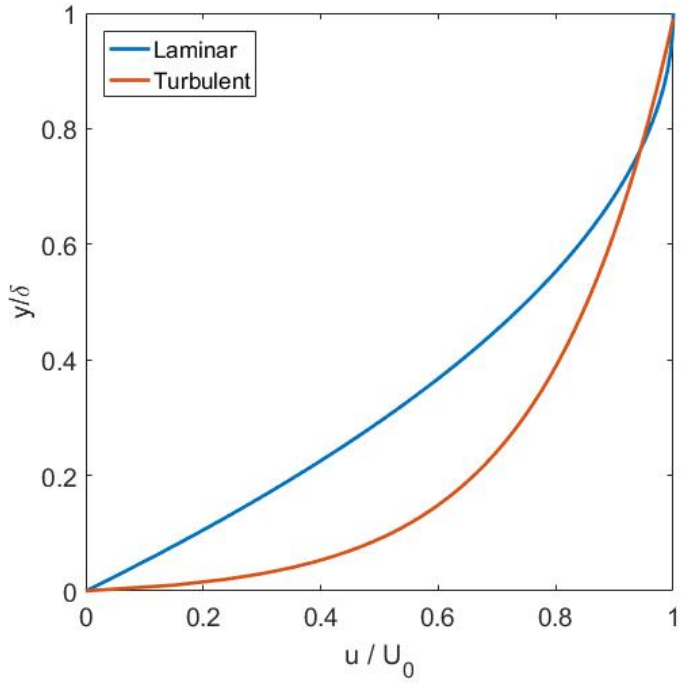

Figure 2.2: Velocity profile [8]

of a turbulent boundary layer differs from the laminar one. It can be seen from 2.2 that the velocity profile is bigger because of friction between flow and the plate.
Therefore is useful to divide the boundary layer in 2 regions: the first one near the wall and dominated by the viscous effects and the other, far from the wall and dominated by the turbulent stress. In order to do that, it is necessary to define a characteristic velocity, which is suitable for both inner and external region and a viscous length.

To study a turbulent boundary layer like the one in figure 2.3 it useful to take in account some other variables such as: the inner velocity u^+ and the inner scaled distance y^+. Them are defined as:

$$u^+ = \frac{u}{U_\tau} \tag{2.9}$$

$$y^+ = yRe_\tau \tag{2.10}$$

Where Re_τ is the Reynolds number based on the friction velocity.

After this assumptions is possible to derive a "*Law of The Wall*" that is the mathematical derivation of the evolving flow that try to predict the value of every physical variables along the wall normal distance of the boundary layer.
The inner layer so can be divided into 3 parts, depending on characteristics and distance:

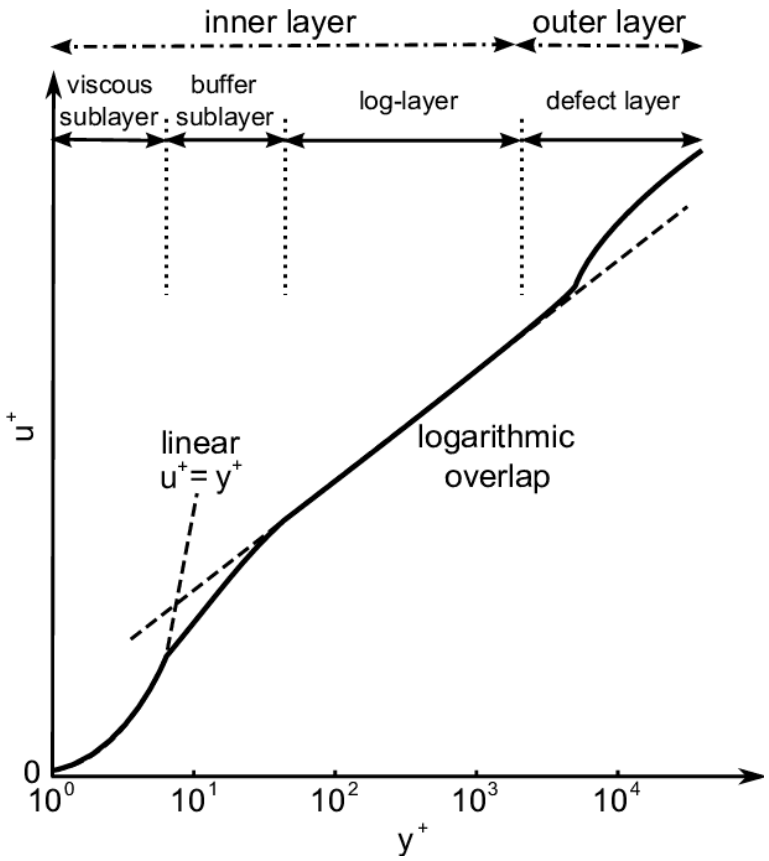

Figure 2.3: Boundary layer regions on a flat plate

- Viscous sub-layer: $y^+ < 5$
- buffer layer: $5 < y^+ < 30$
- log-layer: $30 < y^+ < 100$

all this regions are characterized by mathematical law such,for the viscous sub-layer:

$$y^+ = u^+ \tag{2.11}$$

log-law region:

$$u^+ = \frac{1}{k} log(y^+) + B \tag{2.12}$$

while the buffer layer is a transition region.
k is defined as a Von Karmann constant and is usually $k = 0.41$ and $B = 5.1$
The outer layer instead follows the "$Defect - law$" defined as:

$$\frac{U - \overline{u}}{u_\tau} = B_1 - \frac{1}{k} log(y^+) \tag{2.13}$$

These formulae are useful to predict the behaviour of the boundary layer as the flow goes on. Obviously the are only approximations and there are lot of corrections depending on the case.

2.4 Compressible turbulent boundary layer

Generally the viscosity is avoided but in supersonic and even more, in hypersonic flows it has to be considered.
What differs from subsonic flows is the important role of the thermal field. If a body is immersed in a flow field it will exchange heat based on the temperature difference.
The heat flux:

$$q = -k\frac{\partial T}{\partial y} \tag{2.14}$$

has in general low values of thermal conductivity "k" so to be important the temperature gradient has to be high $\nabla T = (T_\infty - T_w)$; in which T_∞ is the total temperature of the unperturbed flow and T_w is the temperature of the body or wall temperature.
So, the first equation becomes:

$$q = -k\frac{(T_\infty - T_w)}{\delta_T} \tag{2.15}$$

These kind of problems involve coupling between kinematic and thermal field solutions. In order to solve this problem it is possible to start from the Navier-Stokes equations where also the gravitational force is considered:

$$\begin{cases} \frac{D\rho}{Dt} + \rho\nabla\cdot\mathbf{V} = 0 \\ \rho\frac{D\mathbf{V}}{Dt} + \nabla p = \mu\nabla^2\mathbf{V} + (\lambda+\mu)\nabla(\nabla\cdot\mathbf{V}) + \rho\mathbf{g} \\ \rho C_p\frac{DT}{Dt} - \frac{Dp}{Dt} = k\nabla^2 T + \mu\phi \end{cases} \tag{2.16}$$

If there is hydrostatic equilbrium then the momentum conservation equation becomes:

$$\nabla p_s = \rho_\infty \mathbf{g} \tag{2.17}$$

By subtracting this one from the equation (6.3) we obtain:

$$\rho\frac{D\mathbf{V}}{Dt} + \nabla p' = \mu\nabla^2\mathbf{V} + (\lambda+\mu)\nabla(\nabla\cdot\mathbf{V}) + (\rho-\rho_\infty)\mathbf{g} \tag{2.18}$$

Now, with non-dimensional parameters it is possible to understand better the relevance of the terms in the equations.

$$\widetilde{x} = \frac{x}{l}, \quad \widetilde{t} = \frac{V_\infty}{l}t, \quad \widetilde{\mathbf{V}} = \frac{\mathbf{V}}{V_\infty}, \quad \widetilde{\rho} = \frac{\rho}{\rho_\infty}, \quad \widetilde{p} = \frac{p'}{\rho_\infty V_\infty^2}, \quad \widetilde{T} = \frac{T}{\Delta T_0} \tag{2.19}$$

By substituting these values into the Navier-Stokes equations we obtain:

$$\begin{cases} \frac{D\widetilde{\rho}}{D\widetilde{t}} + \widetilde{\rho}\nabla\cdot\widetilde{\mathbf{V}} = 0 \\ \widetilde{\rho}\frac{D\widetilde{\mathbf{V}}}{D\widetilde{t}} + \nabla\widetilde{p} = \frac{1}{Re}\left[\nabla^2\widetilde{\mathbf{V}} + \left(1+\frac{\lambda}{\mu}\right)\nabla(\nabla\cdot\widetilde{\mathbf{V}})\right] + \frac{1}{Fr^2}(\widetilde{\rho}-1)\mathbf{j} \\ \widetilde{\rho}\frac{D\widetilde{T}}{D\widetilde{t}} = \frac{1}{PrRe}\nabla^2\widetilde{T} + Ec\frac{D\widetilde{p}}{D\widetilde{t}} + \frac{Ec}{Re}\widetilde{\varphi} \end{cases} \tag{2.20}$$

where **j** is the unit vector along the direction of the gravitational force. The non-dimensional numbers are:

Reynolds Number $Re = \frac{V_\infty l}{\nu}$

Froude Number $Fr = \frac{V_\infty}{\sqrt{gl}}$

Prandtl number $Pr = \frac{\mu C_p}{k}$

Eckert number $Ec = \frac{V_\infty^2}{C_p \Delta T_0}$

Reynolds number represents the ratio between inertial and viscous forces, Froude number between inertial and gravitational forces. Prandtl number is a characteristic of the fluid itself, and it represents the ratio between the momentum diffusivity and the thermal diffusivity.
Now is possible to subdivide the possible cases in 3 parts:

- $M_\infty < 0.3$, low velocity flows
  Here is possible to neglect the dependency of density from pressure and temperature. The Froude number is high so the buoyancy force can be neglected, even the Eckert can be avoided cause it is enough small this mean that dissipation and compression terms can be neglected. The resultant governing equations are so:

$$\begin{cases} \nabla \cdot \widetilde{V} = 0 \\ \frac{D\widetilde{V}}{D\widetilde{t}} + \nabla \widetilde{p} = \frac{1}{Re} \nabla^2 \widetilde{V} \\ \frac{D\widetilde{T}}{D\widetilde{t}} = \frac{1}{PrRe} \nabla^2 \widetilde{T} \end{cases} \tag{2.21}$$

- $0.3 < M_\infty < 1$, intermediate flow speed
  In this case we are dealing with compressible flow but is still possible to neglect the temperature and density dependency.
  The compressible term can't be avoided due to the Eckert Number, now of order 1. These flows contain a $\Delta T_a \simeq 50K$. The equations becomes:

$$\begin{cases} \frac{D\widetilde{\rho}}{D\widetilde{t}} + \rho \nabla \cdot \widetilde{\mathbf{V}} = 0 \\ \widetilde{\rho} \frac{D\widetilde{\mathbf{V}}}{Dt} + \nabla \widetilde{p} = \frac{1}{Re} \left[\nabla^2 \widetilde{\mathbf{V}} + \left(1 + \frac{\lambda}{\mu}\right) \nabla (\nabla \cdot \widetilde{\mathbf{V}}) \right] \\ \widetilde{\rho} \frac{D\widetilde{T}}{D\widetilde{t}} = \frac{1}{PrRe} \nabla^2 \widetilde{T} + Ec \frac{D\widetilde{p}}{D\widetilde{t}} \end{cases} \tag{2.22}$$

- $M_\infty > 1$, high velocity flows In this case the the value of ΔT_a rises rapidly so it can not be neglected. The temperature also has an important role in fact, the value of viscosity and conductivity depends from it: $\mu(T)$, $k(T)$.
  The kinematic field depends from the thermal one, them need to be solved at the same time.
  Froude number can be negelcted.

2.5 Governing Equations

The energy equation can be simplified due to the fact that the boundary layers thicknesses (thermal and kinematic) are small compared to the characteristic dimension of the body.
Let's consider a bi-dimensional field and avoiding the variability of μ and k.

$$\widetilde{\rho}\left(\widetilde{u}\frac{\partial\widetilde{T}}{\partial\widetilde{x}}+\widetilde{v}\frac{\partial\widetilde{T}}{\partial\widetilde{y}}\right)=\frac{1}{PrRe}\left(\frac{\partial^2\widetilde{T}}{\partial\widetilde{x}^2}+\frac{\partial^2\widetilde{T}}{\partial\widetilde{y}^2}\right)+Ec\left(\widetilde{u}\frac{\partial\widetilde{p}}{\partial\widetilde{x}}+\widetilde{v}\frac{\partial\widetilde{p}}{\partial\widetilde{y}}\right)+\frac{1}{Re}Ec\ \widetilde{\phi} \tag{2.23}$$

In order to simplify this equations, incompressible analysis has to be taken in account and his results, in particular:

- $\widetilde{v}\sim\widetilde{\delta}$
- $\frac{\partial\tilde{p}}{\partial\tilde{y}}\sim\widetilde{\delta}$
- $Re\sim\frac{1}{\widetilde{\delta}^2}$
- $y\sim\widetilde{\delta}$
- $y\sim\widetilde{\delta_T}$

By considering the order of magnitude and after some simplifications the final dimensional equations for a compressible, 2D, steady flow are:

$$\begin{cases}\frac{\partial(\rho u)}{\partial x}+\frac{\partial(\rho v)}{\partial y}=0\\ \rho\left(u\frac{\partial u}{\partial x}+v\frac{\partial u}{\partial x}\right)=\frac{\partial}{\partial y}\left(\mu\frac{\partial u}{\partial y}\right)-\frac{dp}{dx}\\ \rho C_p\left(u\frac{\partial T}{\partial x}+v\frac{\partial T}{\partial y}\right)=\frac{\partial}{\partial y}\left(k\frac{\partial T}{\partial y}\right)+u\frac{dp}{dx}+\mu\left(\frac{\partial u}{\partial y}\right)^2\end{cases} \tag{2.24}$$

The previous equations are valid only for laminar compressible flow. In order to study turbulent compressible flow the Reynolds analogy has to be imposed, this will be explained in the next chapter.

2.6 Recovery Temperature

It's worth noticing that the total temperature is the max value of all the system, it is the stagnation temperature. In the case of adiabatic wall, the total temperature is the temperature at which the wall is, because at the wall the conditions of adherence and impermeability are imposed. In this case:

$$T^0=T+\frac{u^2}{2C_p} \tag{2.25}$$

or better:

$$\frac{T^0}{T}=1+\frac{\gamma-1}{2}M^2 \tag{2.26}$$

Anyway, the total temperature is reached at the wall, where the viscous stress are very significant. The previous formula can be modified in order to have better results or prediction of the temperature profile into the boundary layer such as:

$$\frac{T^0}{T} = 1 + r\frac{\gamma - 1}{2}M^2 \tag{2.27}$$

where "r" is the recovery factor defined as:

$$r = \frac{T_{aw} - T_\infty}{T_{0\infty} - T_\infty} \tag{2.28}$$

The recovery factor is the ratio between the temperature rise due to friction and the one caused by the adiabatic compression. The overall situation is like the one in the next figure:

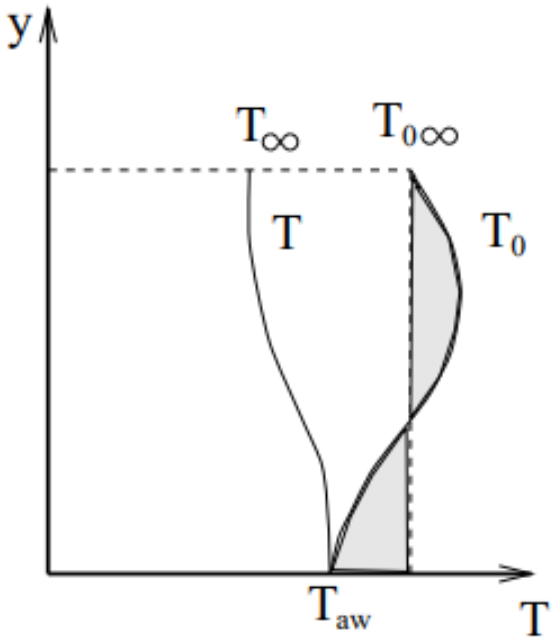

Figure 2.4: Temperature profile

In figure 2.4 the evolution of temperature is shown. Is worth noting that the 2 grey areas are the same so the temperature T_0 has a medium constant value and the T_{aw} is less then the $T_{0\infty}$.

Chapter 3

Large Eddy Simulation

Turbulent flows are always different, a way to understand better their behaviour is to study their boundary layer.
Especially it can be divided in 2 parts: inner layer and outer layer. Every regions has his own problems to discover, describe and modeling.
The inner layer can be divided in 2 sub region:

- inner layer
- log-law region

The first one represent the nearest part of the plate in which the viscous phenomena are important, the second one where neither the viscous effects nor the large-scale boundary geometry effects are dynamically important. To study this problem we can use a DNS (Direcr Numerical Solution) in which we can analyze every little scale of the problem but it costs too much as computational power, we can use a LES, in which we consider only the bigger eddies but not the little ones.
There is another way to study them that uses the precision of a LES for the outer layer and models the inner part with a "LAW OF THE WALL". This derives from mathematical formulations that try to predict the behaviour of the flow in the region nearest to the plate,[19]. The prediction of the characteristics involves not only the velocity but also the temperature, density, viscosity and so on...
This technique is know as WMLES (Wall Model LES).

There are also difficulties on numerical experiments cause as more a certain precision is needed as more the computational cost increases.
Nowadays there 3 main approaches:

- DNS = *Direct Numerical Solutions*, this approach resolves directly the Navier-Stokes equations, is the most accurate but also the most expansive in terms of computational cost. This method is not applicable for industrial application due to the cost.
- LES = *Large Eddy Simulation*, this approach consists on resolve the smallest scale/turbulent scale and to model the smaller one (sub-grid scale=SGS). In this way is possible to maintain a good precision with a minor computational cost. This method have different ways to be applied that will be explained later
- RANS = *Reynold Averaged Navier − Stokes*, in this case the flow is assumed to be a sum of a mean field and a fluctuation. In this way the simulation has significantly reduced cost but also the precision.

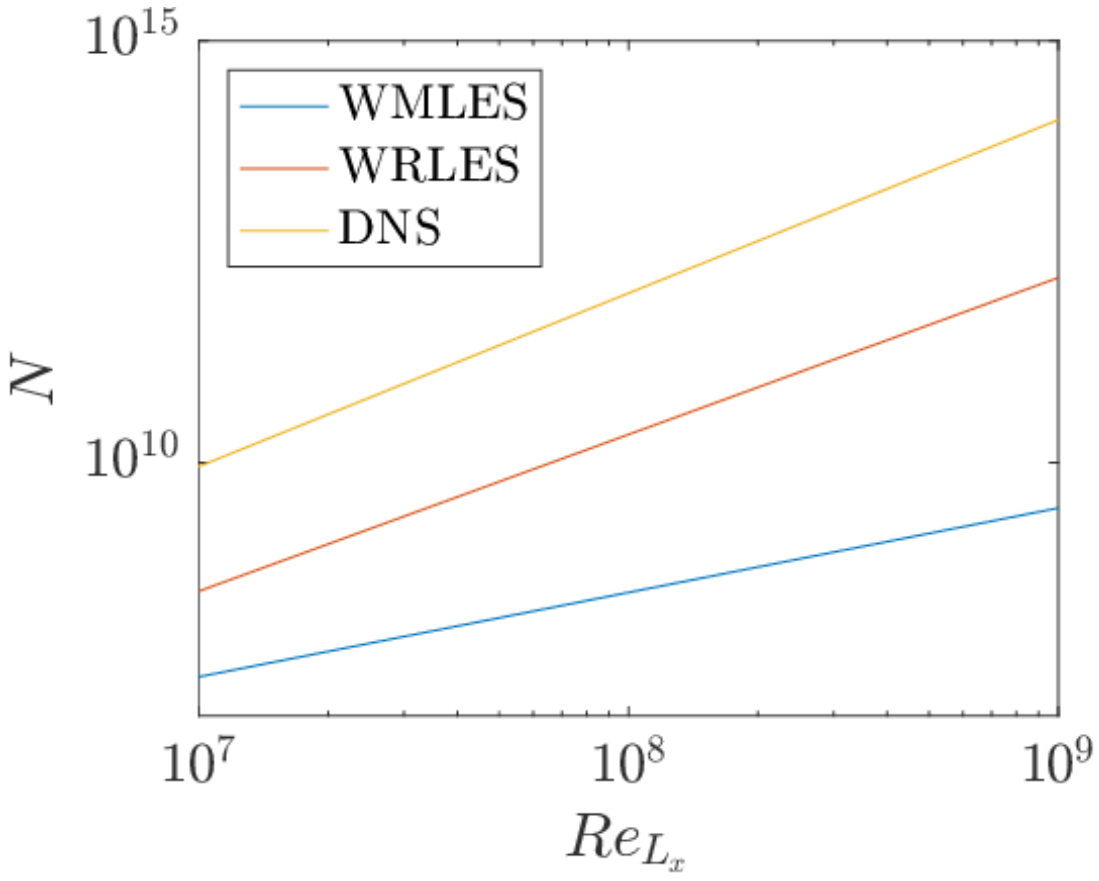

Figure 3.1: Comparison between WM-WR-DNS grid points requirement,[12]

3.1 LES

The actual trend is to use LES, also for industrial application, due to their compromise on cost-precision.
The statistical studies of turbulent compressible flows starts with the averaging or the filtering process. This yields to a mathematical decomposition, in particular the flow f variable is decomposed into an averaged part $\overline{f}$ and a fluctuating or sub-filtered part f'. In general it can be written as [3]:

$$f(x,t) = \overline{f}\ (x,t) + f'(x,t) \tag{3.1}$$

All the filters used in the LES technique are low pass filters since the aim is to cut all the frequencies above the threshold and resolve only the biggest eddies. These filters can however be divided into two classes:

- Explicit filters: the signal is explicitly transformed by the filter. In order to do that, the Δx_i grid spacing must be less than the threshold used in the filter δ. Such filters can be:

  - Gaussian Filter
  $$G_\Delta(r) = \left(\frac{6}{\pi\Delta^2}\right)^2 exp\left(-\frac{6r^2}{\Delta^2}\right) \tag{3.2}$$

  - Top-Hat Filter
  $$G_\Delta(r) = \frac{1}{V_\Delta}\mathcal{H}\left(\frac{\Delta}{2} - r\right) \tag{3.3}$$

- Implicit filters: the filtering is implicitly done by the grid

Nowadays we use the average decomposition of Favre which is focused on density-weighted variables that is in the form:

$$\widetilde{f} = \frac{\overline{\rho f}}{\overline{\rho}} \tag{3.4}$$

where any filtering process can be applied, so this yields:

$$f(x,t) = \widetilde{f}\ (x,t) + f''(x,t) \tag{3.5}$$

In the large eddy simulation methods, these filtered variables are the resolved scale motions.
In order to develop the equations for the resolved or mean motions for compressible turbulent flows, is first applied the conservation equations and then we use the Favre filtering process that yields to:

$$\frac{\partial\overline{\rho}}{\partial t} + \frac{\partial}{\partial x_j}(\overline{\rho u}_j) = 0 \tag{3.6}$$

Now the equation (3.6) is applied and we find:

$$\frac{\partial \overline{\rho}}{\partial t} + \frac{\partial}{\partial x_j}(\overline{\rho}\widetilde{u}_j) = 0 \tag{3.7}$$

The filtered compressible non-dimensional Navier-Stokes equations, taking into account the definition (3.5) becomes:

$$\begin{cases} \frac{\partial \overline{\rho}}{\partial t} = -\frac{\partial}{\partial x_j}(\overline{\rho}\widetilde{u}_j) \\ \frac{\partial(\overline{\rho}\tilde{u}_i)}{\partial t} + \frac{\partial}{\partial x_j}(\tilde{u}_i\overline{\rho}\tilde{u}_j) = -\frac{\partial \overline{p}}{\partial x_i} + \frac{\partial \overline{\sigma}_{ij}}{\partial x_j} - \frac{\partial \overline{R}_{ij}}{\partial x_j} \\ \frac{\partial(\overline{\rho}\tilde{E})}{\partial t} + \frac{\partial(\tilde{u}_j\overline{\rho}\tilde{H})}{\partial x_j} = \frac{\partial(\overline{u_i\sigma_{ij}})}{\partial x_j} - \frac{\partial \overline{q}_j}{\partial x_j} - \frac{\partial \overline{Q}_j}{\partial x_j} \end{cases} \tag{3.8}$$

where the averaged/filtered viscous stress tensor and turbulent stress tensor are written as:

$$\overline{\sigma}_{ij} = \overline{2\mu\left(S_{ij} - \frac{1}{3}S_{kk}\delta_{ij}\right)} \tag{3.9}$$

$$\overline{R}_{ij} = \overline{\rho}(\widetilde{u_i u_j} - \widetilde{u}_i\widetilde{u}_j) \tag{3.10}$$

3.2 The Reynolds Analogy

The Reynolds Analogy is popularly known to relate turbulent momentum and heat transfer. That is because in a turbulent flow the transport of momentum and the transport of heat largely depends on the same turbulent eddies. In particular it relates the velocity to the temperature. This theory was then extended to compressible flows. Busemann and Crocco independently obtained a relation for compressible laminar boundary layers by assuming unity Prandtl number (Pr, for air $Pr \simeq 0.7$). Their derivations were extended to turbulent boundary layers by Van Driest. These studies show that the mean temperature is a quadratic function of the mean velocity. Every variables is expressed in terms of mean values:

$$\frac{T}{T_\delta} = \frac{T_w}{T_\delta} + \frac{T_{c\delta} - T_w}{T_\delta}\frac{u}{u_\delta} + \frac{T_\delta - T_{c\delta}}{T_{c\delta}}\left(\frac{u}{u_\delta}\right)^2 \tag{3.11}$$

In this equation T is the temperature, u is the streamwise velocity, w denotes the wall, δ denotes the boundary layer edge.

Some improvements have been made from Waltz, with the assumption of constant mixed Prandtl number and temperature is assumed a function of only u, [15]. Subsequent improvements were made [16], the so called "GRA=generalized Reynolds analogy", in which also the recovery factor is considered.

The equation becomes:

$$\frac{T}{T_\delta} = \frac{T_w}{T_\delta} + \frac{T_{rg} - T_w}{T_\delta}\frac{u}{u_\delta} + \frac{T_\delta - T_{rg}}{T_{c\delta}}\left(\frac{u}{u_\delta}\right)^2 \tag{3.12}$$

There the quadratic behaviour is the same as the previous relations but by adopting a general recovery factor r_g.

3.3 Wall-Stress Model

The Wall Stress Model used assumes equilibrium between convection and pressure gradient. Under this assumption [4], the momentum and energy equations of Navier-Stokes can be simplified and written as:

$$\frac{d}{dy}\left[(\mu_{wm} + \mu_{t,wm}\frac{dU_{wm}}{dy})\right] = 0 \tag{3.13}$$

$$\frac{d}{dy}\left[c_p\left(\frac{\mu_{wm}}{Pr} + \frac{\mu_{t,wm}}{Pr_{t_wm}}\right)\frac{dT_{wm}}{dy}\right] = -\frac{d}{dy}\left[(\mu_{wm} + \mu_{t,wm})\,U_{wm}\frac{dU_{wm}}{dy}\right] = 0 \tag{3.14}$$

and the wall-model eddy viscosity is taken as:

$$\mu_{t,wm} = k\rho\sqrt{\frac{\tau_w}{\rho}}y[1 - exp(-y^+/A^+)]^2 \tag{3.15}$$

in which:

$$D = [1 - exp(-y^+/A^+)]^2 \tag{3.16}$$

is called Van Driest dumping function.
All these equations are solved over the region $0 \leq y \leq h_{wm}$ as described below.
With regard to hypersonic flows the heat transfer is important and generally it is calculated with the Fourier's law:

$$q_{wall} = \lambda_w \frac{dT}{dy}\Big|_{wall} \tag{3.17}$$

In this work are considered compressible flows this mean that the energy equation plays an essential role so, after some derivations [10], is possible to rewrite the previous equation as:

$$q_w = \left(U_{wm}\tau_{wm} + c_p\frac{\mu_{t,wm}}{Pr_{t,wm}}\frac{dT}{dy}\right)_{y=h_{wall}} \tag{3.18}$$

This describes the heat flux as a sum of aerodynamic heating and the turbulent heat transport at h_{wall}.

3.4 WMLES approach

Basically, the WMLES paradigm foresees that the true nature of turbulence in the inner zone is characterized using a model that determines the desired instantaneous wall-shear stress τ_w and heat flux q_w, whereas in the outer zone the eddies are resolved directly, like in a LES. These quantities are then given back to the LES field. This way, the correct wall shear stress and heat flux can be imposed on the wall.

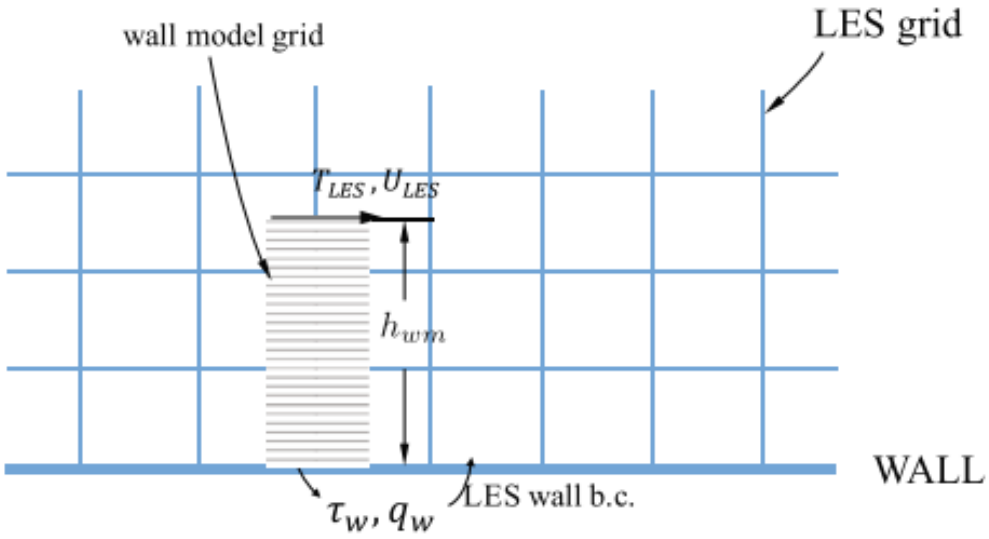

Figure 3.2: WMLES approach, [5]

The principle of wall-stress-modeled LES if the wall-model is decoupled from the LES grid. Instantaneous boundary layer with overlaid LES grid. The wall-model models the flow in a layer of thickness h_{wm}; it is fed instantaneous velocity and temperature information from the LES, and returns the instantaneous wall stress and heat flux to the LES, which then uses these as the wall boundary condition. Generally, The wall-model thickness h_{wm} is chosen to fall within the log-layer.

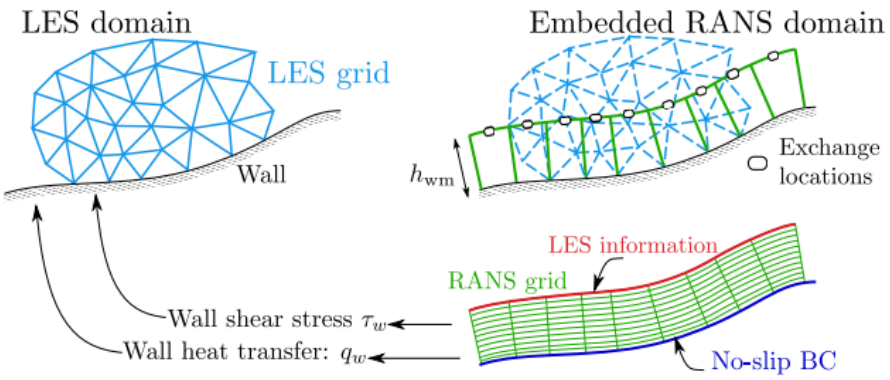

Figure 3.3: LES Vs WMLES, image taken from [4]

In figure 3.3 is shown the Implementation of wall-stress-modeled LES where the wall-model is decoupled from the LES grid in complex geometries. The wall-modeled thickness h_{wm} is specified independently from the LES grid, which necessitates interpolation from the LES grid to the top of the wall-modeled layer.

Chapter 4

Numerical approach

With a view to solve the Navier-Stokes equations it is needed a specific numerical treatment for the problem. These equations are made of 2 terms: convective and diffusive, and the way to solve them is by using a finite difference technique (FD). Different schemes can be used everyone with pros and cons, afterwards, it will be briefly described.

4.1 Finite differences schemes

The main idea is to approximate the derivative of a function by using incremental ratios.
A field can be taken in account as a function of space and time: $\phi(x,t)$. Now, to study it is necessary to discretize through a grid and, forasmuch as a flow is 3D the discretisation must be done in x,y,z by using nodes: n_x,n_y,n_z.
Now the field can be written as: $\phi_i = \phi(x_i, y_j, z_k, t)$ and the nodes used to compute the derivative is called Stencil.
For the first derivative:

$$\frac{d\phi(i)}{dx_i} \simeq \frac{1}{\Delta x} \sum_{s=s_{min}}^{s=s_{max}} \alpha_s^1 \phi_{i+s} \tag{4.1}$$

and second derivative:

$$\frac{d^2\phi(i)}{dx_i^2} \simeq \frac{1}{\Delta x^2} \sum_{s=s_{min}}^{s=s_{max}} \alpha_s^2 \phi_{i+s} \tag{4.2}$$

The stencil can be centered or unbalanced to the left or to the right and they are so called: centered, upwind or downwind.
If the scheme used is not centred, then, in addition to the dispersion error, the modified wave number shows an imaginary part, this gives an additional term in the equation [6]. This term is called "artificial dissipation" and depends on the sign of the velocity; it can decreases the signal magnitude or vice versa increases until the simulation becomes unstable. In both cases the quality of the solution is reduced. On the other hand there the centered schemes cannot be implemented for supersonic/hypersonic flows due to the strong gradients and, shock waves

cause them give rise to numerical oscillation and instability.
Consequently, for this type of work the upwind/downwind schemes are implemented.

4.2 WENO

WENO (Weighted Essentially Non Oscillatory) methods are used for studying problem in which there is a discontinuity. In order to do that, these techniques use a discretization (computational stencil) of a discontinuous function and then choose the points in which the function is more regular.

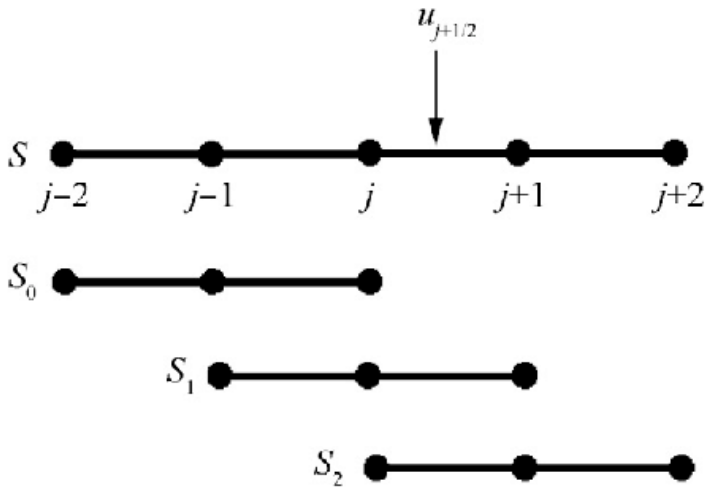

Figure 4.1: WENO 5 implementation scheme, image taken from [7]

To understand the dynamics of these methods, in figure 4.1 is represented a WENO 5 technique. These points (stencils) WENO scheme uses a 5 points stencil and 3 sub-stencil (S_0, S_1, S_3). It weights them in a particular way. The weights depend on the local smoothness of the function. Smoothness measurements cause stencils that span large flow field gradients to have relative small weights; any candidate stencil containing a shock receives a nearly zero weight.
Based on this, practically, the discontinuity is avoided. As mentioned above this scheme uses an upwind/downwind method in order to evolve the shock wave.
To solve the problem we consider:

$$\frac{\partial \mathbf{F}_j}{\partial x} \simeq \frac{1}{\Delta x}\left(\hat{\mathbf{f}}_{j+1/2} - \hat{\mathbf{f}}_{j-1/2}\right) \tag{4.3}$$

in the case of a conservative approximation of the advection term.
It is needed to compute the flux at $u_{j+1/2}$ here, a standard procedure of 5 steps is applied [6]:

1. First step consists in calculating the mean flux variables at the interface $j + 1/2$

2. Second step instead, the eigenmatrices of the Jacobian are calculated ($\mathbf{L}_{j+1/2}, \mathbf{R}_{j+1/2}$).

3. Here a flux splitting technique is applied in order to subdivide the flow function in 2 terms: one with positive propagation, the other with the negative one.

$$\mathbf{f}^{\pm}_{j+1/2} = \frac{1}{2}\mathbf{L}_{j+1/2}(\mathbf{F}_j \pm |\lambda_{max}|\mathbf{U}_j) \tag{4.4}$$

   where $\mathbf{f}^{\pm}_{j+1/2}$ correspond to the split fluxes projected upon the characteristic directions. λ_{max} is the maximum eigenvalue and represents the maximum velocity of propagation.

4. In the fourth step is an application of WENO interpolation i each characteristic direction. Every sub-stencil has his own polynomial expression, so in a WENO 5 we have 3 different values. Afterwards them are recombined in a non-linear ways such as:

$$\mathbf{f}_{j+1/2} = \sum_{k=0}^{2} \mathbf{w}_k \mathbf{q}^{(k)+}_{j+1/2} \tag{4.5}$$

   where $\mathbf{w}_k$ are the non linear coefficients.

5. At the end, once that $\mathbf{f}^{\pm}_{j+1/2}$ have been computed are recombined and moved to the physical space.

4.3 TENO

Generally there lot of difficulties on simulating turbulent flows. In particular increasing WENO order is not always beneficial.
In particular WENO techniques are too dissipative for direct simulations of turbulence and lack robustness when very-high-order versions are applied to complex flows.
So, a family of high-order targeted ENO (TENO) schemes which are applicable for compressible-fluid simulations involving a wide range of flow scales. As explained before WENO schemes exploit a weighted average of approximations from all candidate stencils. Based on the smoothness indicators, the weights are designed to recover the ENO property for capturing discontinuities and to restore the background linear schemes in smooth regions of the solution. Noticing that classical WENO schemes fail to recover the formal fifth-order accuracy near critical points. The main idea for these new schemes is:

- Create a high-order reconstruction by assembling a set of low-order upwind-biased candidate stencils with incremental width. The new scheme can gradually degenerate to third order, according to local flow features, thus avoiding the problem of multiple discontinuities.
- Stronger scale-separation formulation is designed to isolate discontinuities from high wavenumber physical fluctuations.
- A candidate stencil either is applied with optimal weight, or eliminated entirely when it contains a genuine discontinuity with certain strength.
- Optimization results in an order degeneration of one, but provides favorable spectral properties satisfying the dispersion–dissipation relation.

Briefly, a set of candidate stencils has to be derived for the high-order reconstruction. A new approach, by which the high-order full stencil is constructed from low-order stencils with incrementally increasing width. Each candidate stencil with one end node at x_i contains at least one-point upwind. For the TENO scheme the three-point candidate stencil S0 avoids the crossing of discontinuities and thus can be singled out as smooth candidate stencil to contribute to the final reconstruction. Since practical numerical experiments reveal that fifth-order WENO scheme is robust for such configurations, the TENO schemes also can recover the robustness of fifth-order WENO scheme even for very-high-order reconstructions.

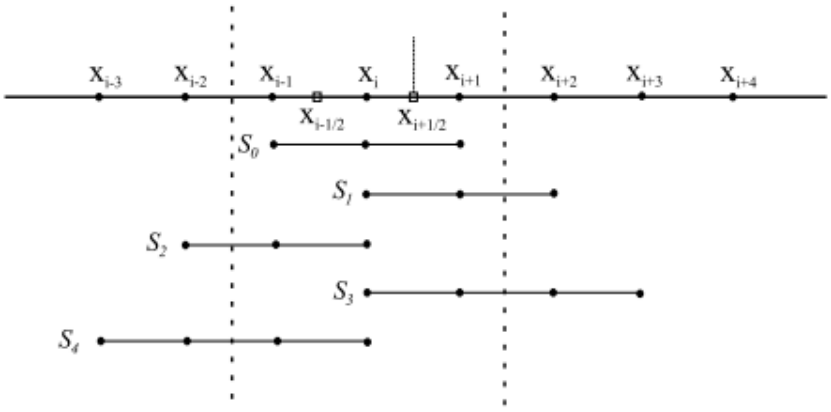

Figure 4.2: TENO-7 implementation scheme, [20]

In this way we have a better robustness, in particular for all cases, the TENO schemes produce mostly better results than previous solutions with a unique fit of parameters. These techniques can capture discontinuity better, more sharply. With regard to efficiency it is practically the same.
For high-resolution schemes, high-order accuracy is not the most important issue, e.g. high odd-order upwind scheme may still be unnecessarily dissipative. Even the TENO5 and scheme exhibit good spectral properties and shock-capturing capabilities. This last one is the method used for the test battery..

4.4 Ducros sensor

When we are dealing with supersonic or hypersonic flows in impossible to avoid the compressibility effects. In particular when we are simulating a flow with these features we need to introduce a way to detect and study a shock wave.
In particular it is necessary to detect a priori the region where shock waves are located and then applying the WENO scheme and limiting it in these locations.
For these problems a sensor can be used, in particular an improved version of the Ducros sensor, [18].
This shocks detector is expressed as:

$$\theta = max\left(-\frac{div(\mathbf{u})}{\sqrt{(div(\mathbf{u}))^2 + rot(\mathbf{u})^2 + \varepsilon}}, 0\right) \tag{4.6}$$

After the selection of a sensor a proper threshold must be chosen in order to distinguish the shocked from the smooth region. If the minimum value is reached then the WENO technique is activated.

Chapter 5

Turbulence

The majority of flows are turbulent, this phenomena brings with it several problems. First of

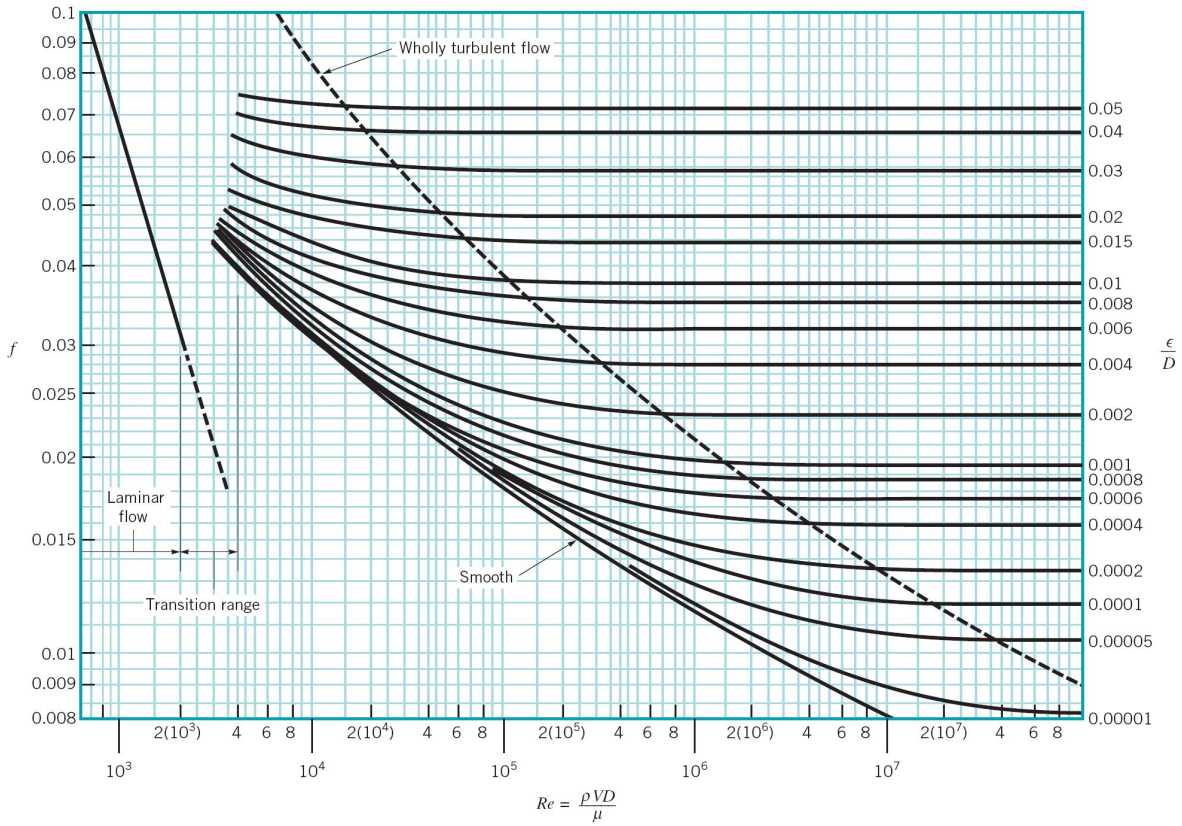

Figure 5.1: Moody Diagram

all if we observe a flow if Reynolds exceeds the value of 10^4 the friction increases rapidly, there is a transition form laminar to turbulent flow. If the Reynolds number continues to increase then the friction will assume a constant value.
Others properties than can be observed from experiments, in particular as the Reynolds increases symmetry is lost and vorticity rises.

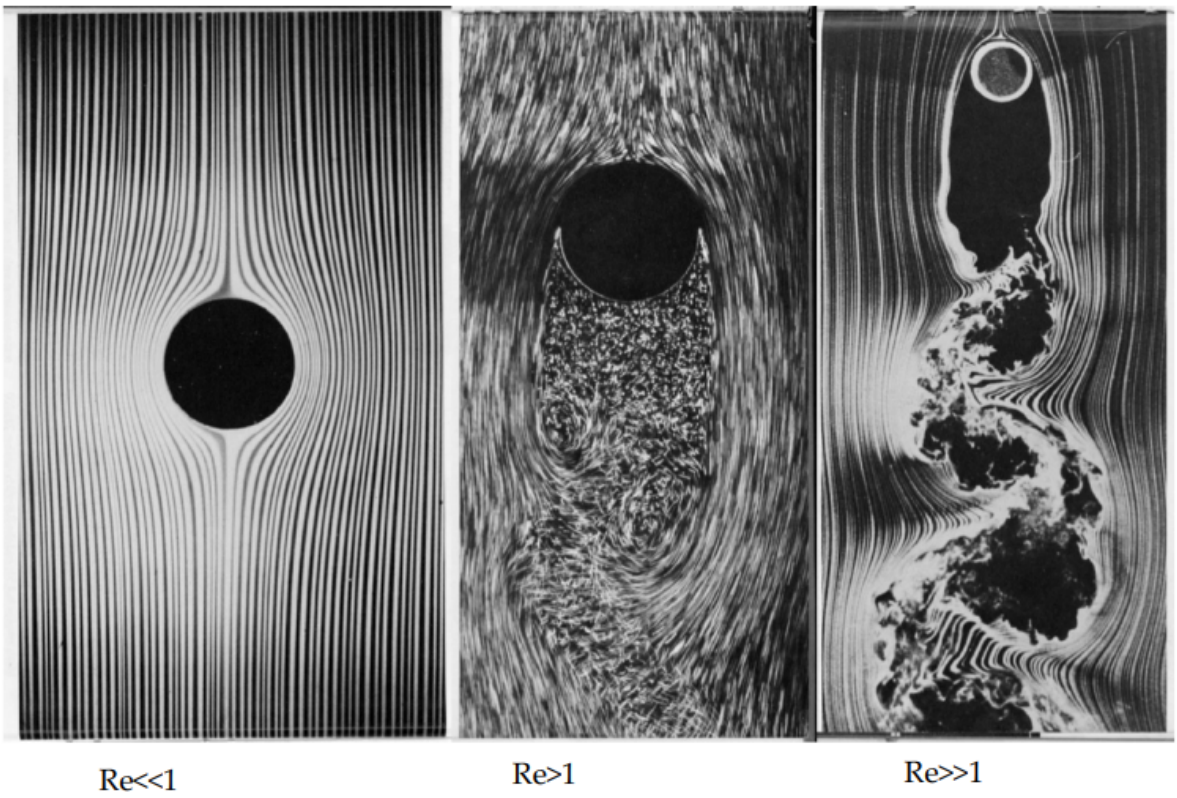

Figure 5.2: Moody Diagram

Another problem of turbulent flows is their close dependence from boundary conditions. In particular if we repeat the same experiments lots of times the result would we all different, this is due to the small perturbations (even non-measurable) causing what is known as deterministic chaos.
A way to study turbulent flows is by subdividing them in 2 parts:

1. **Mean** field:
    * Recovers symmetries
    * Does not varies with space and time
    * Seems like a laminar field
2. **Instantaneous** field:
    * is fluctuating in space and time
    * 3D behaviour
    * High spatial/temporal variations in every scales
    * The gradients increases as Reynolds increases

In order to study these problems an important step was made by Richardson by using the concept of *energy cascade*,[17].

5.1 Energy Cascade and Kolmogorov hypoteses

The main idea is considering the turbulence to be composed of *eddies* of different sizes. The definition of eddies is not precise but it is conceived to be a turbulent motion, localized within a region of size ℓ.
The eddies in the largest size range are characterized by the length scale ℓ_0 which is comparable to the flow scale $\mathcal{L}$.
In Richardson hypothesis the large eddies are unstable and break up, and transfer their energy to some smaller eddies. These smaller eddies follow a similar break-up process, and transfer their energy to other smaller eddies. This energy cascade – in which energy is transferred to successively smaller and smaller eddies – continues until the Reynolds number is sufficiently small that the eddy motion is stable, and molecular viscosity is effective in dissipating the kinetic energy.
Kolmogorov hypothesized that:

- The small-scale turbulent motions ($\ell_0 \ll \ell_0$) are statistically isotropic.
- In a turbulent flow at sufficiently high Reynolds number, the statistics of the small-scale motions ($\ell \ll \ell_{EI}$) have a universal form that is uniquely determined by ν and ϵ.
- In every turbulent flow at sufficiently high Reynolds number, the statistics of the motions of scale ℓ_0 in the range $\ell_0 \gg \ell \gg \eta$ have a universal form that is uniquely determined by ϵ, independent of ν.

Where the ν is the kinematic viscosity and, ϵ is the energy dissipation.
Now is possible to divide the e the scales of turbulent motion in three main parts:

1. **Energy-containing range**: here the turbulent energy is introduced into the system, it it represented by P or production term
2. **Inertial sub range**: this part is dominated by inertial forces. There is low dissipation but the energy is transferred from the largest scales to the smallest
3. **Dissipation range**: the scales are smaller than the Kolmogorov scale. In this range the viscous effects dissipate the turbulent kinetic energy into heat

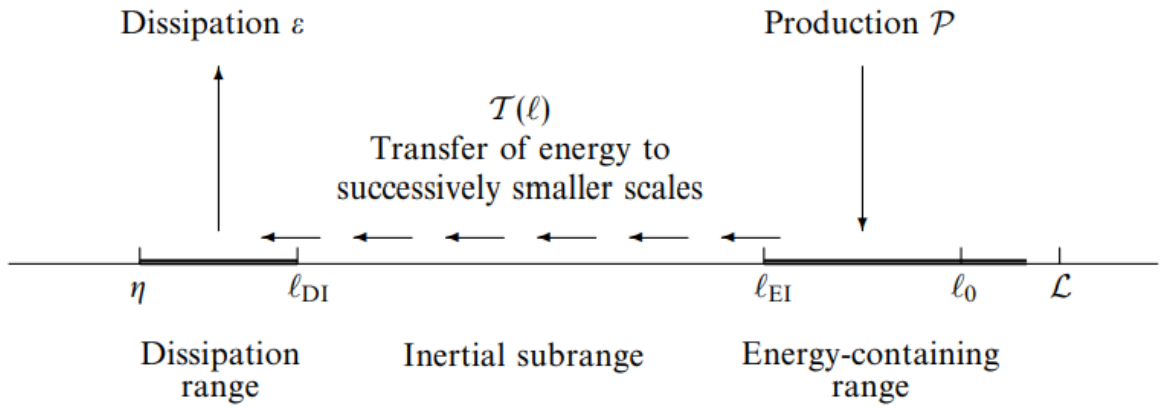

Figure 5.3: A schematic diagram of the energy cascade at high Reynolds number

5.2 Spectrum Energy

From Kolmogorov theory is possible to understand better the energy distribution among the eddies of different sizes.
In particular form the first Kolmogorov hypothesis in the universal equilibrium range the spectrum is a universal function of ϵ and ν.
From the second hypothesis it follows that, in the inertial range the spectrum is:

$$E(k) = C\epsilon^{2/3}k^{-5/3} \tag{5.1}$$

This is valid only if the Reynolds number is high enough that the energy containing and dissipation scales are well separated.

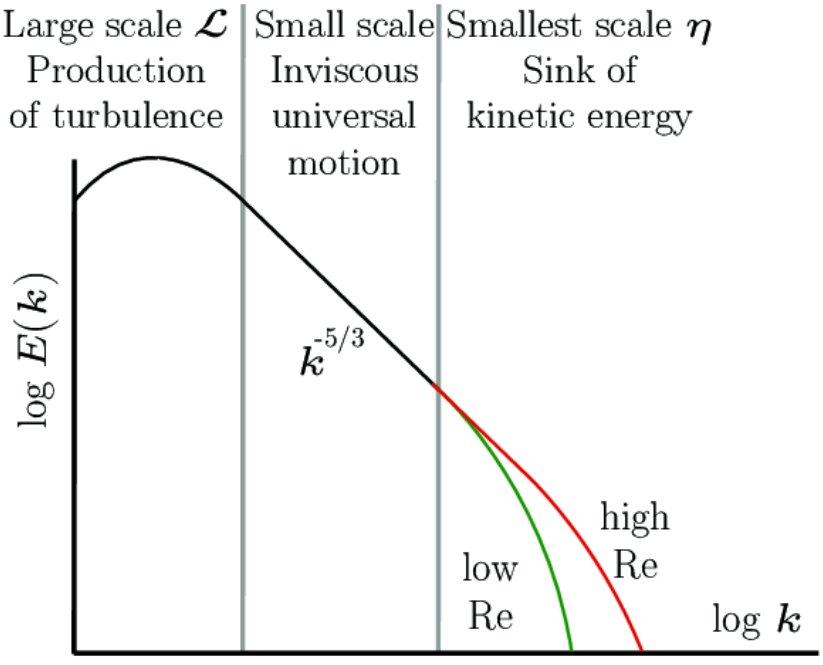

Figure 5.4: Turbulent kinetic energy decay

Chapter 6

Study case

6.1 Uranos

Simulations were performed by using URANOS (Unsteady All-Around Navier-StOkes Solver), developed by Francesco De Vanna during his PhD. URANOS is a low-dissipative high-order and high-resolution numerical solver specifically developed for fluid simulation in strong-compressible viscous conditions and able to deal with moving objects at high-Mach numbers, [11].
In order to validate the code, different test were performed. In particular by using different grid resolutions, different value of θ and different schemes.
To be more clear 5 schemes were used, in particular different precision of WENO and TENO techniques:

- WENO 3
- WENO 5
- WENO 7
- TENO-5
- TENO-5A

The values of θ changed from $\theta = 0.0$ to $\theta = 0.1$ in order to study the influence of centered schemes on the reconstruction process of shocks for the different schemes.

6.2 Grids

A wall-modeled LES requires a sufficiently fine grid in order to resolve the turbulent flow. In particular an uniform grid distribution has been used in every directions.

Domain	Point number	Non-dimensional Spacing
$x_{min} = 0,\ x_{max} = 90$	384	$\Delta x^+ = 105.47$
$y_{min} = 0,\ y_{max} = 10$	64	$\Delta y^+ = 35.15$
$z_{min} = -3,\ z_{max} = +3$	64	$\Delta z^+ = 42.188$

Table 6.1: Grid 1, parameters of a Wall-modeled boundary layer

In table 6.1 is shown the grid parameters used for the first battery of test, then the value of θ was changed and different schemes have been used.
Another battery of tests were performed by increasing the grid resolution, in particular:

Domain	Point number	Non-dimensional Spacing
$x_{min} = 0,\ x_{max} = 90$	512	$\Delta x^+ = 79.10$
$y_{min} = 0,\ y_{max} = 10$	96	$\Delta y^+ = 23.44$
$z_{min} = -3,\ z_{max} = +3$	96	$\Delta z^+ = 28.12$

Table 6.2: Grid 2, parameters of a Wall-modeled boundary layer

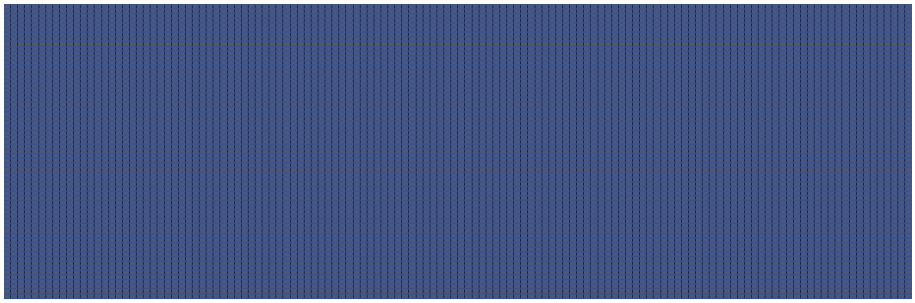

Figure 6.1: WMLES grid distribution, uniform grid representation

The LES simulation were performed with the following data:

Domain	Point number	Non-dimensional Spacing
$x_{min} = 0,\ x_{max} = 90$	576	$\Delta x^+ = 70.31$
$y_{min} = 0,\ y_{max} = 10$	128	$\Delta y^+ = 1.21$
$z_{min} = -3,\ z_{max} = +3$	192	$\Delta z^+ = 13.77$

Table 6.3: Grid 3, parameters of the LES

In this case, a wall-resolved technique has been used, the grid is not uniform but it has more resolution as we get closer to the boundary layer.
This decision was made in order to prove that increasing grid resolution brings better solutions. As far as we are using a WMLES to reduce the computational cost a comparison will be made for the different cases proposed.

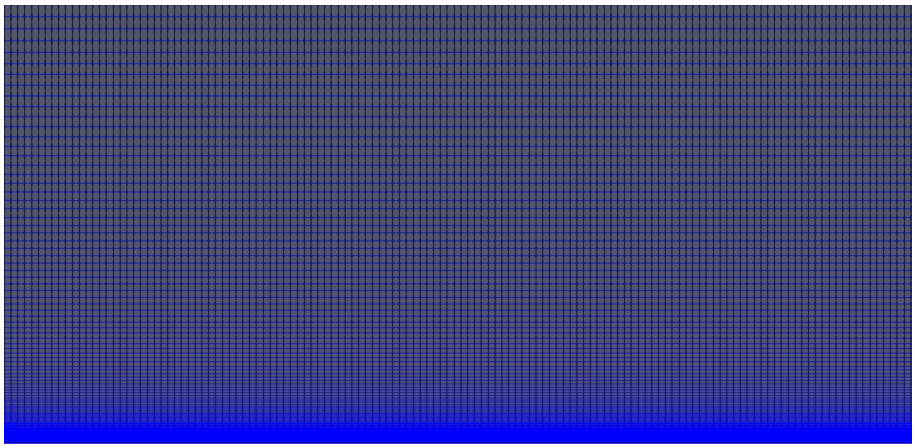

Figure 6.2: LES grid distribution

6.3 Computational cost

All the different cases are here compared in terms of time, to prove that different schemes and different technique can be way to expensive for the same results.

6.3.1 384x64x64

Scheme	Time(dd)
TENO-5	$t \simeq 3.36$
TENO-5A	$t \simeq 3.67$
WENO3	$t \simeq 3.74$
WENO5	$t \simeq 3.93$
WENO7	$t \simeq 3.48$
LES	$t \simeq 9.95$

Table 6.4: Time comparison for each simulation, when $\theta = 0.0$

Scheme	Time(dd)
TENO-5	$t \simeq 3.00$
TENO-5A	$t \simeq 3.25$
WENO3	/
WENO5	$t \simeq 3.50$
WENO7	$t \simeq 3.67$
LES	$t = 9.95$

Table 6.5: Time comparison for each simulation, when $\theta = 0.1$

6.3.2 512x96x96

Scheme	Time(dd)
TENO-5	$t \simeq 5.09$
TENO-5A	$t \simeq 6.36$
WENO3	$t \simeq 4.85$
WENO5	$t \simeq 5.15$
WENO7	$t \simeq 6.00$
LES	$t \simeq 9.95$

Table 6.6: Time comparison for each simulation, when $\theta = 0.0$

Scheme	Time(dd)
TENO-5	$t \simeq 6.02$
TENO-5A	$t \simeq 6.05$
WENO3	/
WENO5	$t \simeq 5.45$
WENO7	$t \simeq 6.80$
LES	$t \simeq 9.95$

Table 6.7: Time comparison for each simulation, when $\theta = 0.1$

As can be seen, the time required for a WMLES is a lot lower than a LES, in particular also the grid refinement has its role. The denser grid has triple the points but only a 50% more computational time while, the LES has 50% more time required compared to a WMLES with more or less the same results, as shown in the next section.

6.4 Results

Here we compare the simulations carried out in order to validate the code URANOS.
For each test the case in which $Re_\tau \simeq 450$ has been considered, and then everything was compared to DNS results from Zang et al. [9], and with the LES results. Comparisons are made for different grids and different values of θ, each case using different schemes.

6.4.1 GRID = 384x64x64

$$\theta = 0.0$$

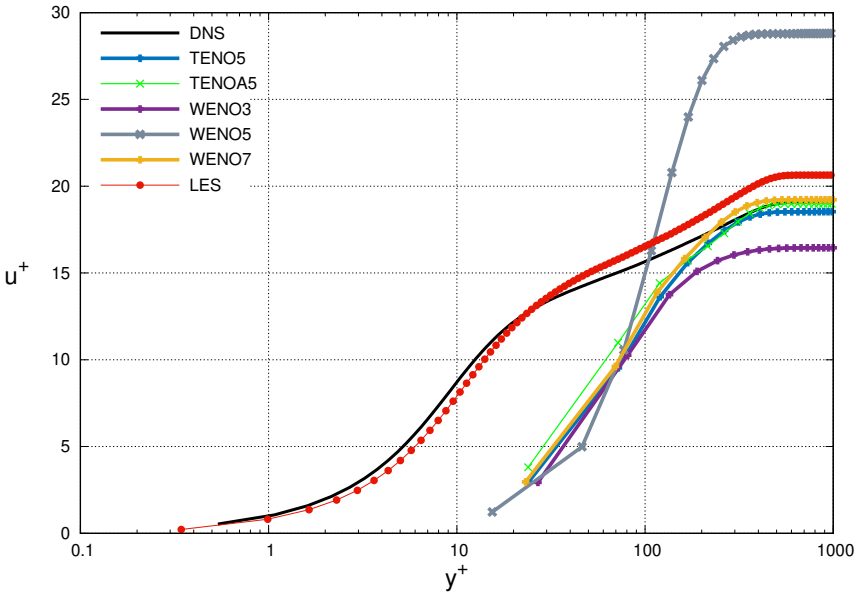

Figure 6.3: Velocity profiles comparison with all the schemes

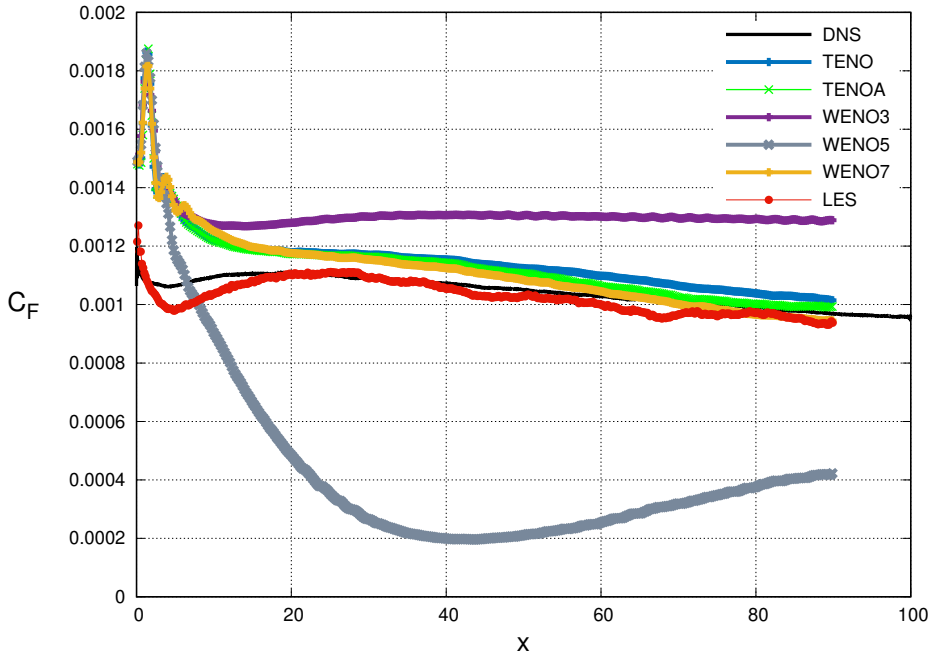

Figure 6.4: Comparison of friction coefficients along the plate

From these analysis we see that the results are not good for the majority of the simulations due to the value of $\theta = 0.0$, in particular only WENO7 and TENO schemes give good results for both variables. As expected, the results from the LES simulation are similar to the DNS ones. The WMLES simulation doesn't give the expected Re_τ, in particular once the flow is steady, it can't reach the value of $Re_\tau \simeq 450$ but it stops at $Re_\tau \simeq 390$. This happens because the dissipation is too high since the Ducros filter is zero.
To prove that, an analysis of Reynolds stresses can be done.
Afterwards, only DNS and WMLES data are compared.

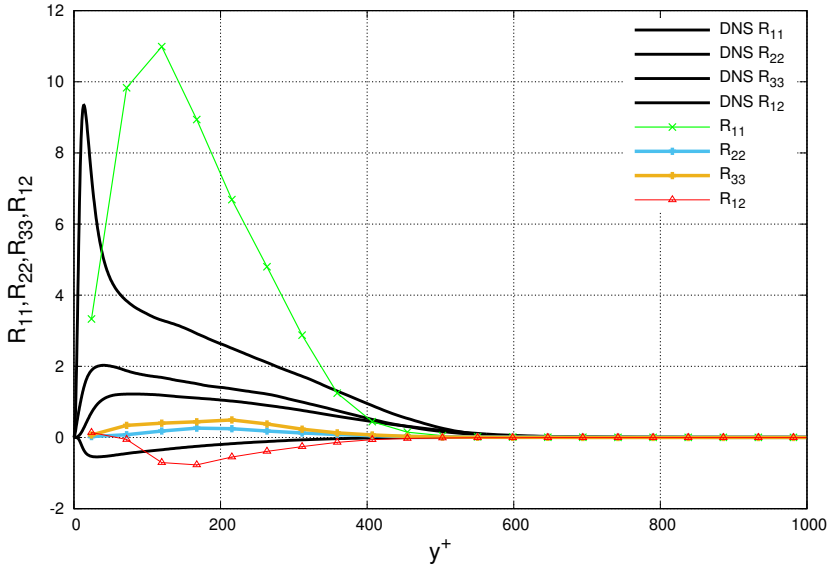

Figure 6.5: Reynolds stresses comparison at $Re_\tau = 420$ function of the wall distance y^+ for TENO5-A scheme.

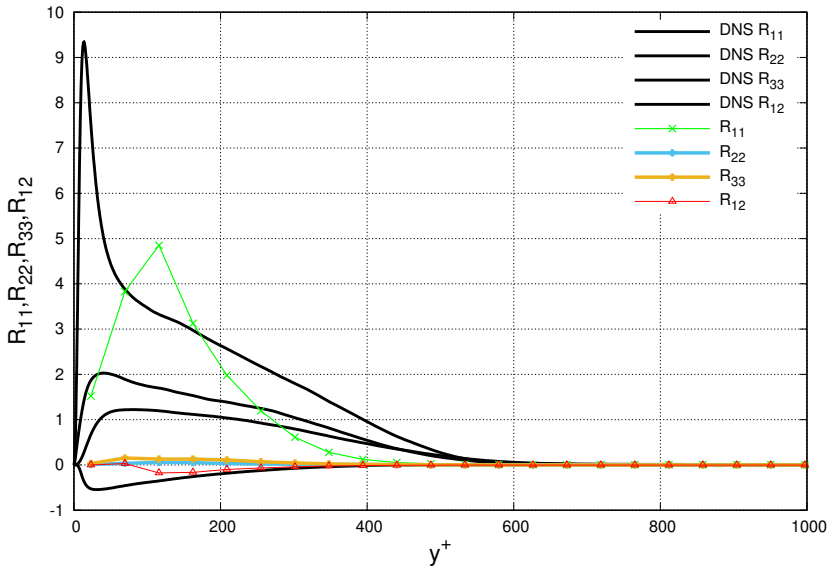

Figure 6.6: Reynolds stresses comparison at $Re_\tau = 390$ function of the wall distance y^+ for WENO 7 scheme.

Up to here the results are not good, the other techniques give the same trend. Even if the velocity profile and the friction coefficients are acceptable, except for WENO 5, the Reynolds stresses are not. Anyway, the TENO5 and TENO5-A techniques seem to give better results. The reason behind these Reynolds stresses results lies in the boundary condition, a value of $\theta = 0.0$ has been imposed so the fluctuations are not captured due to high dissipation of the implemented schemes. In the next tests the sensor is imposed to the valued of $\theta = 0.1$, thus an improvement of the data is expected.

$$\theta = 0.1$$

In these cases the Ducros sensor is activated, so the influence of the shock wave is considered.

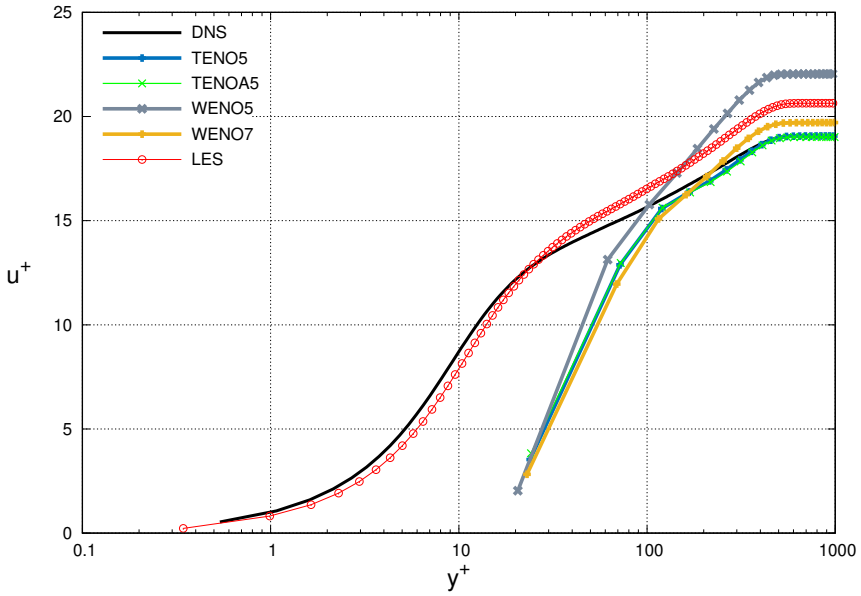

Figure 6.7: Reynolds stresses comparison at $Re_\tau = 450$ function of the wall distance y^+ for all the schemes.

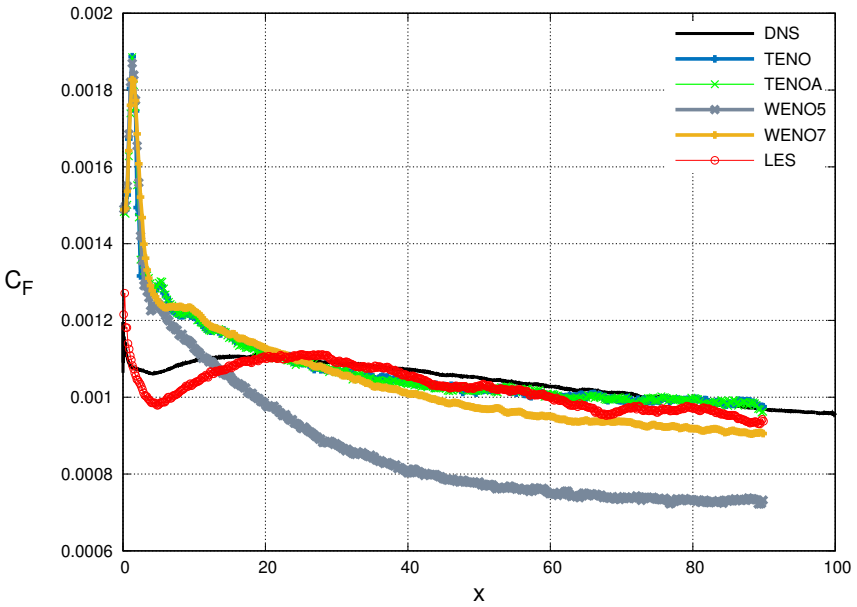

Figure 6.8: Comparison of friction coefficients along the plate

As can be seen, there are better results in every parameter calculated. In particular, we have a strong improvement for the WENO-5 scheme. The missing method here is the WENO3, because of the characteristics of the method itself, since the dissipation is so high that it leads to the annulment of the simulation.

The Reynolds stresses now are compared to the DNS ones, it is expected to see an improvement on their calculation.

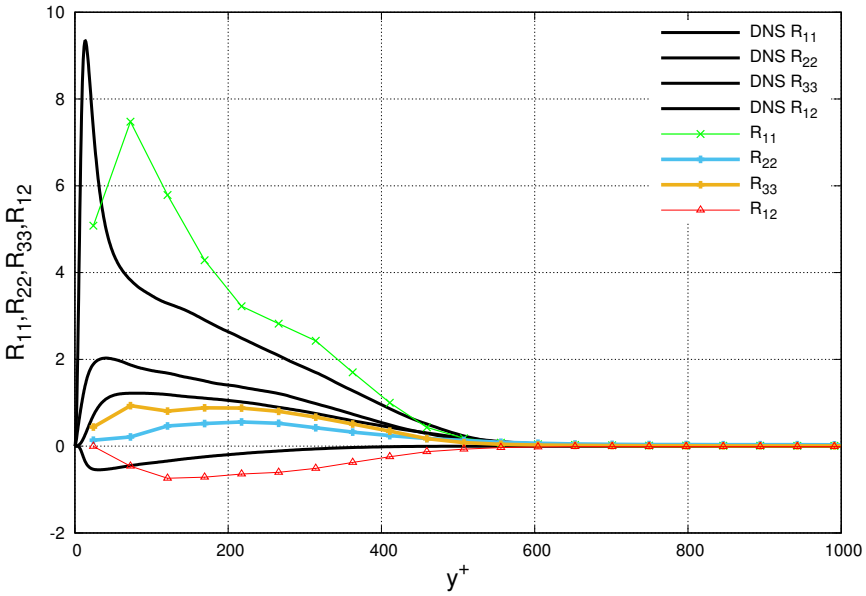

Figure 6.9: Reynolds stresses comparison at $Re_\tau = 450$ function of the wall distance y^+ for TENO5-A scheme

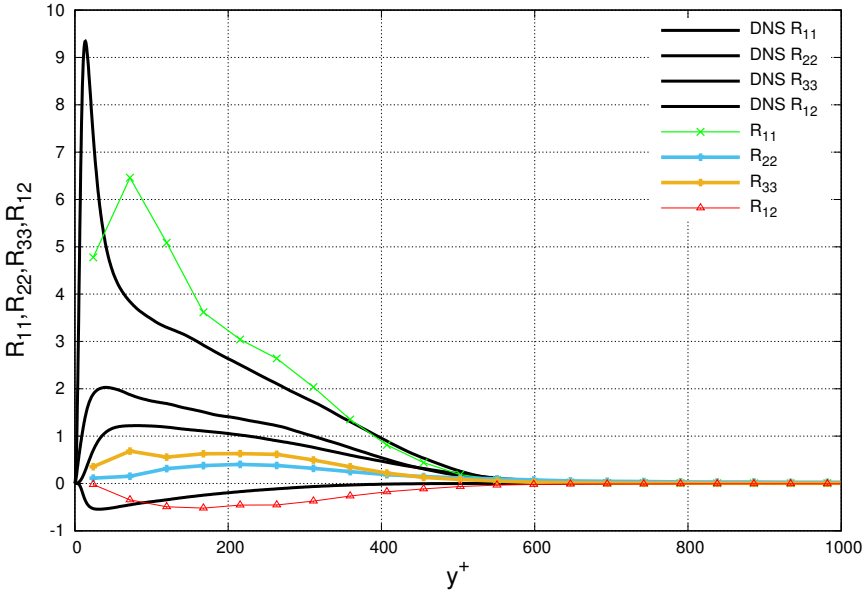

Figure 6.10: Reynolds stresses comparison at $Re_\tau = 450$ function of the wall distance y^+ for TENO5 scheme

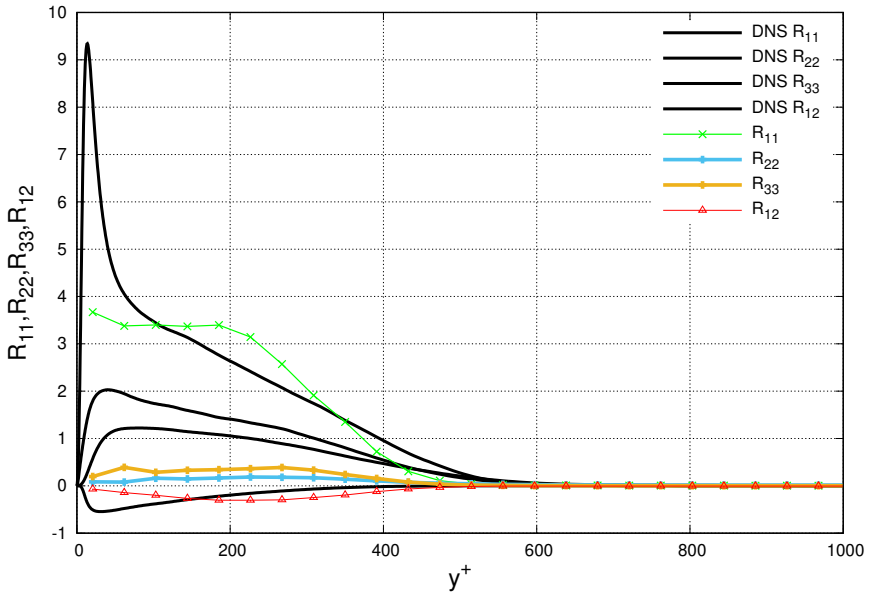

Figure 6.11: Reynolds stresses comparison at $Re_\tau = 450$ function of the wall distance y^+ for WENO-5 scheme

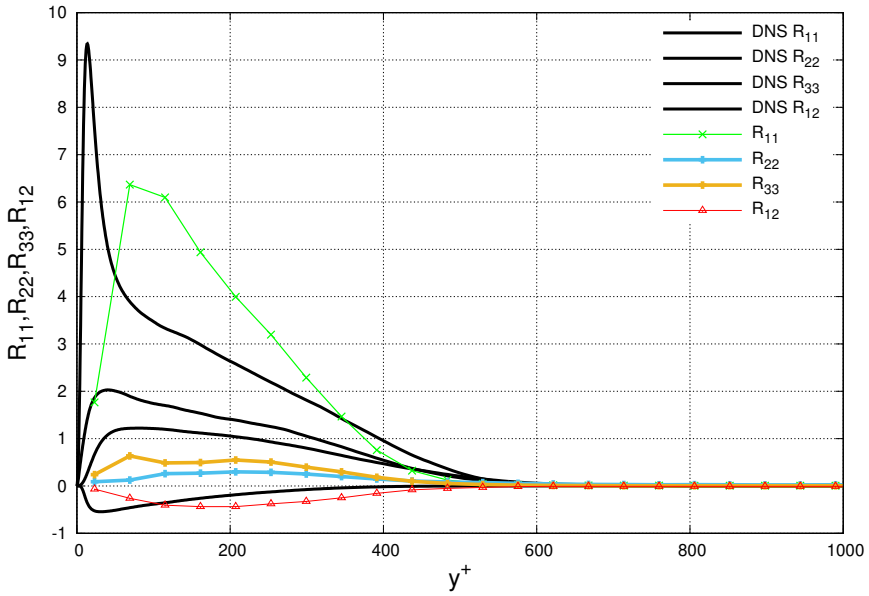

Figure 6.12: Reynolds stresses comparison at $Re_\tau = 450$ function of the wall distance y^+ for WENO-7 scheme

From this test battery it can be seen how increasing the WENO order brings to better results. This includes every type of variable.
Best results are given from TENO5 and TENO5-A schemes.
As regards the WENO3 case, it has a low order of accuracy, so low that it makes the simulation explode. As explained in chapter 4, the more points are used, the more the calculation along the shocks is smoother.
In fact three and five sub-stencils are not sufficient. It can be seen that even though WENO 5 scheme provides results, they are not accurate, only the WENO7 technique is acceptable. As remarked, more sub-stencils imply more accuracy but also more computational cost.
In general, the first part of simulations give bad results because there is a transition part in which the flow is chaotic at the beginning, then it stabilizes itself and becomes steady. This phenomenon is due to the initial condition of the flow, since it requires some time or distance in the x-direction to become a turbulent flow.
The WENO-3 technique has too few sub-stencils to bypass the shocks, in fact the simulation explodes. On the other hand, in the case of $\theta = 0.0$ it gives bad results because only upwind/downwind schemes are implemented. The problem is the high dissipation of the WENO techniques.
In conclusion, we can see that 'filtering' the shocks with the Ducros sensor brings better results. In these cases the fluctuations are better captured, but the methods are not yet convergent.
In order to improve the results, a more refined grid has been used.

6.4.2 GRID = 512x96x96

$$\theta = 0.0$$

In the next test battery only the grid resolution has changed. This was made in order to prove if the grid has an influence on the results.

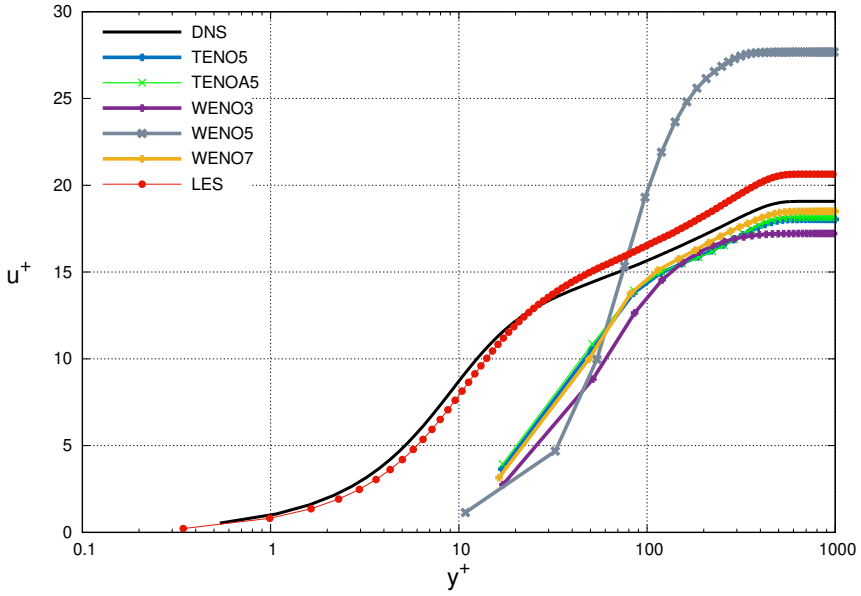

Figure 6.13: Velocity profiles comparison with all the schemes

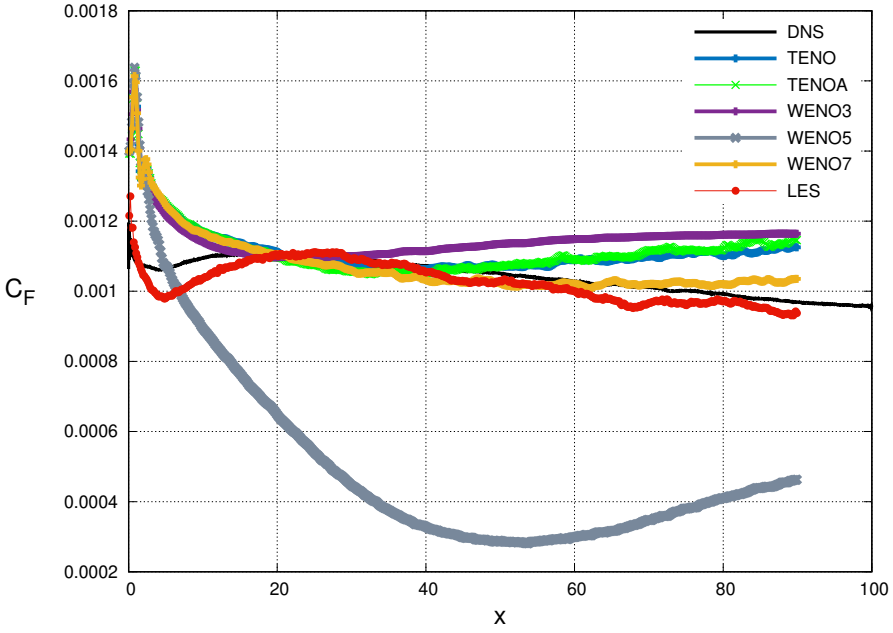

Figure 6.14: Comparison of friction coefficients along the plate

We notice the same trend of the previous results with only a slightly improvement.

As it was done for the previous tests, the Reynolds stresses are compared to the DNS results for every single scheme.

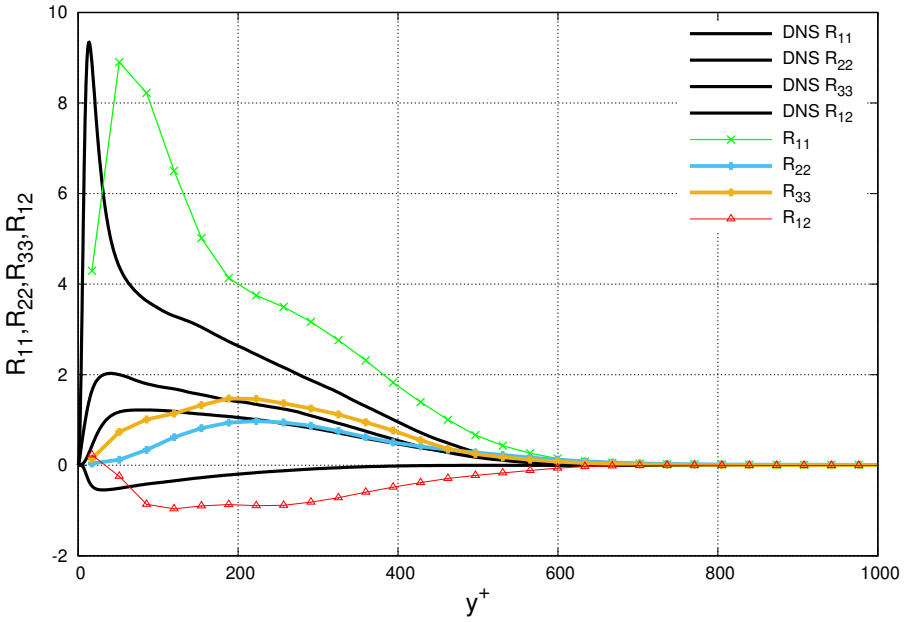

Figure 6.15: Reynolds stresses comparison at $Re_\tau = 450$ function of the wall distance y^+ for TENO5-A scheme.

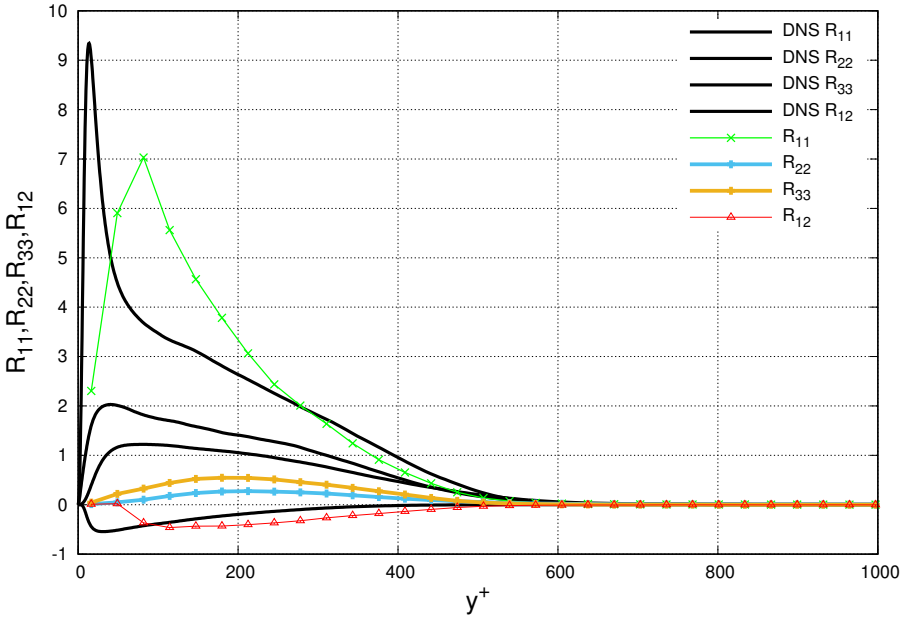

Figure 6.16: Reynolds stresses comparison at $Re_\tau = 450$ function of the wall distance y^+ for WENO-7 scheme.

From these results we can see that, even though the solutions are not correct, they give better results due to the more refined grid. In fact, in these two cases the Reynolds stress components are not 0 or nearly 0, but they give better results. To be more precise, the R_{22} and R_{33} in the final part have the same trend for the TENO scheme. With regard to the TENO-A5 scheme, it has the same results, while the WENO3 and WENO5 do not give good results.
In order to prove that the results improve with the grid and with the value of $\theta = 0.1$, another battery of test has been made.

$$\theta = 0.1$$

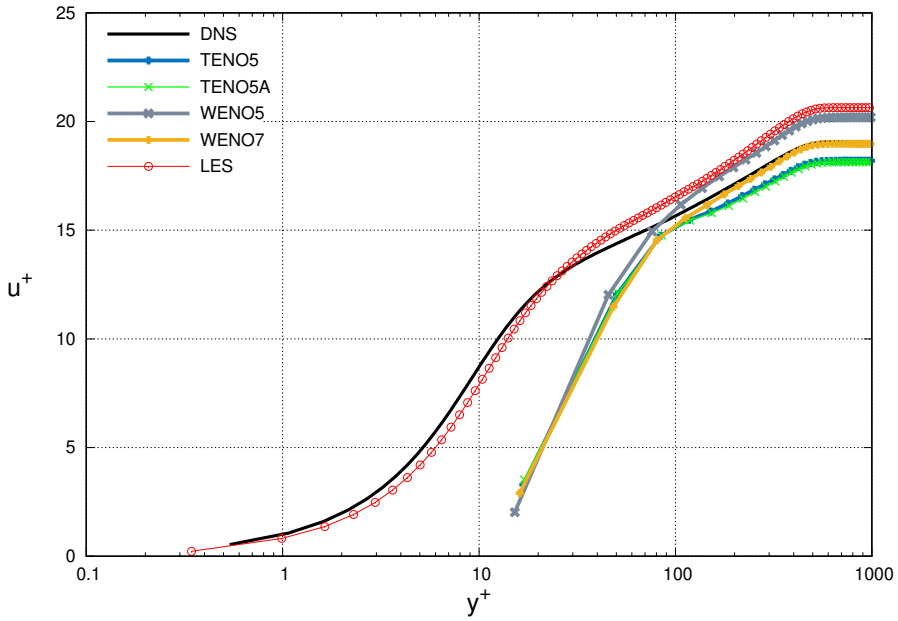

Figure 6.17: Velocity profiles comparison with all the schemes

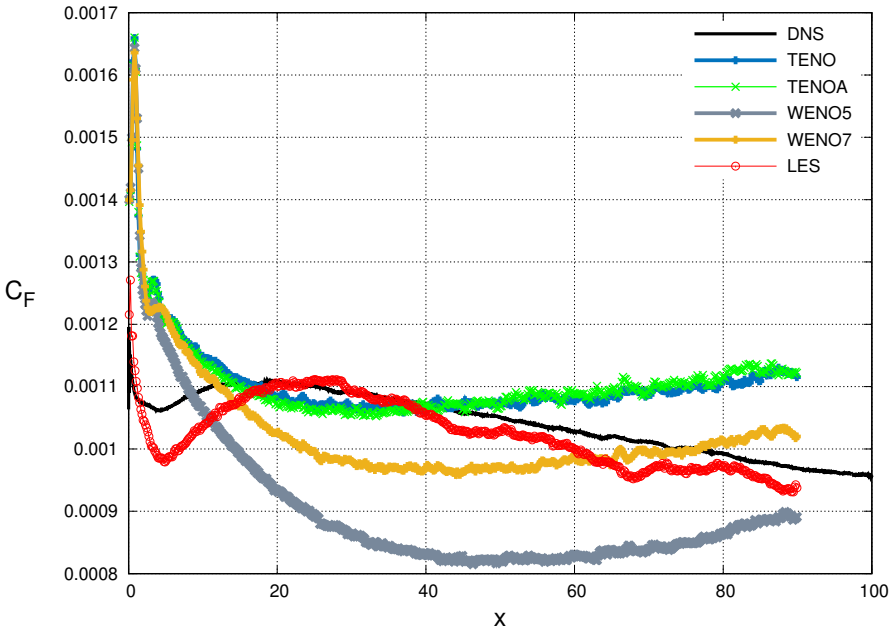

Figure 6.18: Comparison of friction coefficients along the plate

In these conditions we have a great improvement of the results even for WENO5 scheme, even though it gives better data is still not acceptable, the method has too dissipation.

In order to prove that, the reynolds stresses comparison has been made. In this case results are expeted to be improved and valid.

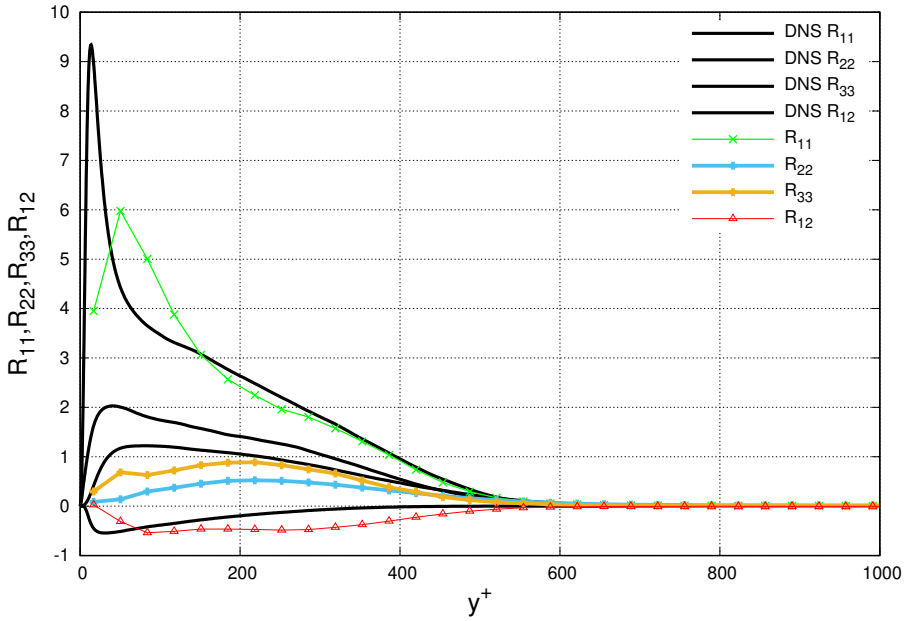

Figure 6.19: Reynolds stresses comparison at $Re_\tau = 450$ function of the wall distance y^+ for TENO-5 scheme.

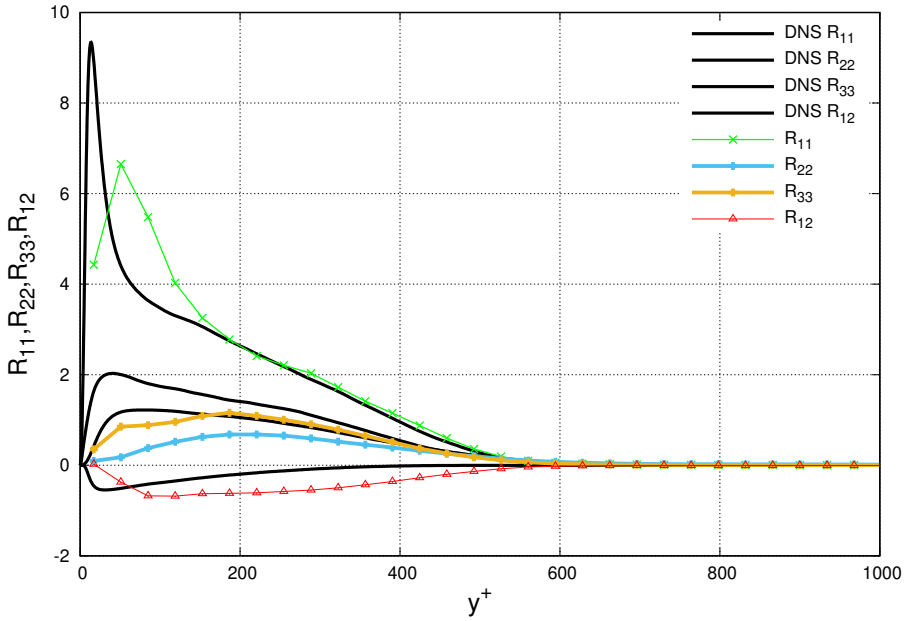

Figure 6.20: Reynolds stresses comparison at $Re_\tau = 450$ function of the wall distance y^+ for TENO-5A scheme.

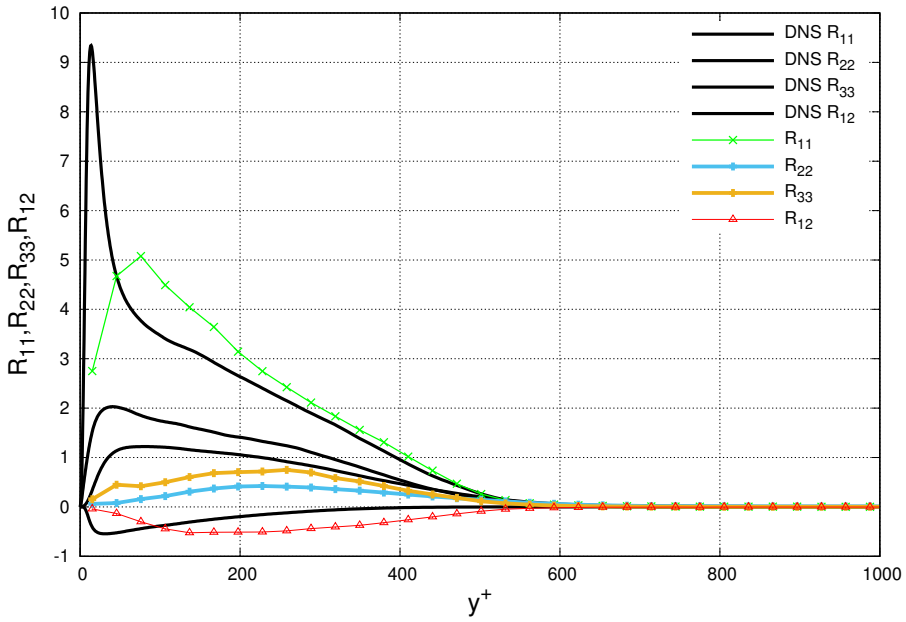

Figure 6.21: Reynolds stresses comparison at $Re_\tau = 450$ function of the wall distance y^+ for WENO-5 scheme.

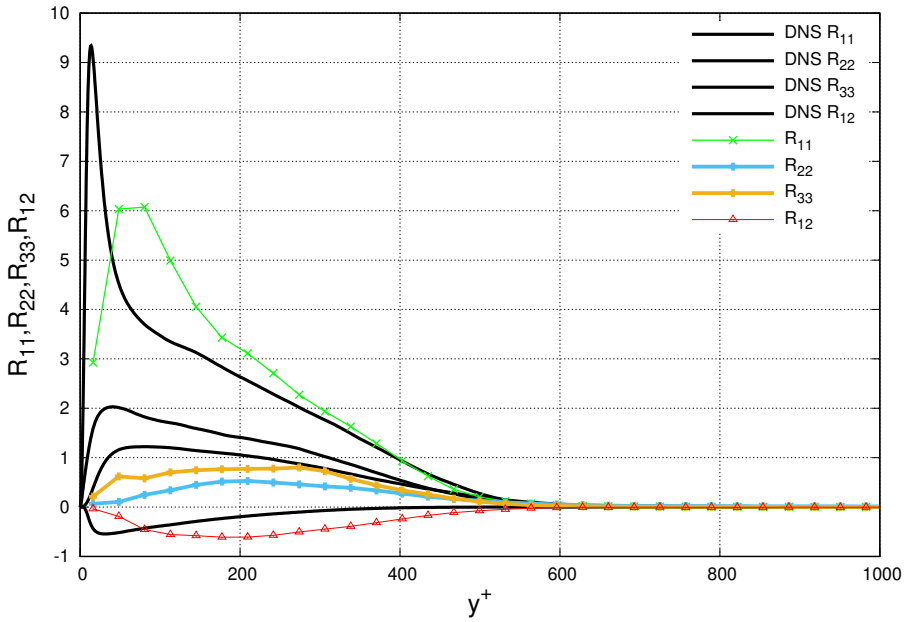

Figure 6.22: Reynolds stresses comparison at $Re_\tau = 450$ function of the wall distance y^+ for WENO-7 scheme.

In this test battery we have similar and different results.
First of all, we have in general better results for every scheme used. In particular, only in this case WENO-5 gives acceptable results for velocity and better data for friction coefficient. This method remains the worst one but with improvement.
WENO-3 again, is not sufficiently accurate to run, as seen in the previous cases it dissipates too much when the shocks interactions are considered.
All the other results are acceptable for velocity and friction coefficient. An important outcome is that the Reynolds stresses are acceptable only in this test battery. In particular it can be observed that TENO schemes capture the R_{11} value well, but also R_{22} and R_{33}, R_{12} is acceptable too.
Another consideration can be made regarding the WENO schemes. They give acceptable results but convergence is reached later, in other words they need more sub-stencils, in fact the results are acceptable from $y^+ \simeq 300/400$ while for the TENO schemes from $y^+ \simeq 150$.
As explained in previous chapters, the TENO technique gives better results because it is less dissipative and it captures the turbulence better with more or less the computational cost.
In addition, the value of theta, by implementing centered schemes, gives better results due to the less dissipation of the finite differences themself.

Chapter 7

Conclusions

This thesis aims to study a hypersonic turbulent flow using the simplest geometry: boundary layer over a flat plate.
Some simulation have been carried out using different grids, different schemes and different parameters.
Particularly, the goal was to find the best way to simulate an hypersonic turbulent flow with a Wall-modeled LES technique. As shown the time required for these type of test is much lower compared to a LES or DNS technique.
Different tests pointed out that grid resolution has an influence, the more refined is the grid the better are the result due to the improved simulation of streaks that govern the dynamic near the wall.
Moreover, a big difference is made from the Ducros sensor that has been studied, especially when activated the simulation sees the shocks better, centered schemes are less dissipative, and their influence so, the fluctuation are well captured and give rise to the Reynolds stresses.
In addition different schemes has been used, from WENO to TENO, each one with different precision orders. Particularly, WENO schemes gives better results as the order increases but the lower ones fail due to high dissipation.
On the other hand, TENO schemes have only one order of precision but are structured for these type of problems, for this reason the results are a lot better in every case proposed. Moreover, the TENO technique has the same computational cost compared to the WENO techniques.
It's worth noticing that the nowadays trend is to use WMLES in order to study complex phenomena due to their low computational cost and their good results. Particularly, the technique is promising for wall turbulent flows and validated.
On industrial application DNS or LES simulation are still too expensive compared to the demands of a company business, which instead could be satisfied by means of a WMLES technique.

Bibliography

[1] Jr. Anderson, J. D. "*Fundamentals of Aerodynamics*". McGraw-Hill, New York, 6th edition, (2017).

[2] Stephen B. Pope, "*Turbulent Flows*", Cornell Uniuersity

[3] Thomas B. Gatski, Jean-Paul Bonnet."*Compressibility, Turbulence and High Speed Flow*", 2nd edition (2013).

[4] Johan LARSSON, Soshi KAWAI, Julien BODART, and Ivan BERMEJO-MORENO. Large eddy simulation with modeled wall-stress: recent progress and future directions. *Mechanical Engineering Reviews*, 3(1):15–00418–15–00418, 2016. doi: 10.1299/mer.15-00418.

[5] Xiang I. A. Yang and Yu Lv. A semi-locally scaled eddy viscosity formulation for LES wall models and flows at high speeds. *Theor. Comput. Fluid Dyn.* (2018) 32:617–627, https://doi.org/10.1007/s00162-018-0471-3.

[6] Francesco De Vanna. Appunti del corso di laboratorio di fluidodinamica computazionale, a.a. 2020/2021.

[7] Interface flux reconstruction method based on optimized weight essentially non-oscillatory scheme. Peixun YU,Junqiang BAI,Hai YANG, Song CHEN, Kai PAN. Aircraft Strength Research Institute of China, Laboratory of Aeronautical Acoustics and Dynamics, Xi'an 710065, (2017).

[8] F. Picano. Lecture of the Course of Aerodynamics 2, University of Padua, a.a.2019/2020.

[9] Chao Zhang, and Lian Duan. Direct Numerical Simulation Database for Supersonic and Hypersonic Turbulent Boundary Layers. Missouri University of Science and Technology. DOI: 10.2514/1.J057296

[10] X. I. A. Yang and J. Urza. Aerodynamic Heating in Wall-Modeled Large-Eddy Simulation of High-Speed Flows.

[11] Francesco De Vanna. A high-resolution fully compressible Navier-Stokes solver for analysis of moving objects at high Mach numbers. (2019)

[12] Haecheon Choi and Parviz Moin. Grid-point requirements for large eddy simulation: Chapman's estimates revisited. Physics of Fluids, 24(1):011702, 2012. doi: 10.1063/1.3676783. URL https://doi.org/10.1063/1.3676783.

[13] Kadeem Dennis, Kamran Siddiqui. The influence of wall heating on turbulent boundary layer characteristics during mixed convection.

[14] Ronald J. Adrian. Hairpin vortex organization in wall turbulence. Laboratory for Energetic Flow and Turbulence, Department of Mechanical and Aerospace Engineering, Arizona State University, Tempe, Arizona 85287

[15] WALZ, A. 1966 Stromungs-und Temperaturgrenzschichten ¨ . Braun (translation in Boundary Layers of Flow and Temperature, MIT Press, 1969).

[16] You-Sheng Zhang, Wei-Tao Bi1, Fazle Hussain and Zhen-Su She. A generalized Reynolds analogy for compressible wall-bounded turbulent flows. Department of Mechanical Engineering,Texas Tech University, Lubbock, TX 79409-1021, USA.

[17] Lewis Fry Richardson. Weather prediction by numerical process. Cambridge university press, 2007.

[18] Ducros, F. (1999). Large-eddy simulation of the shock/turbulence interaction. Journal of Computational Physics, 152:517—-549.

[19] Wall-modeled large-eddy simulation of a separated flow over the NASA wall-mounted hump. By G. I. Park

[20] A family of high-order targeted ENO schemes for compressible-fluid simulations. Lin Fu, Xiangyu Y. Hu , Nikolaus A. Adams